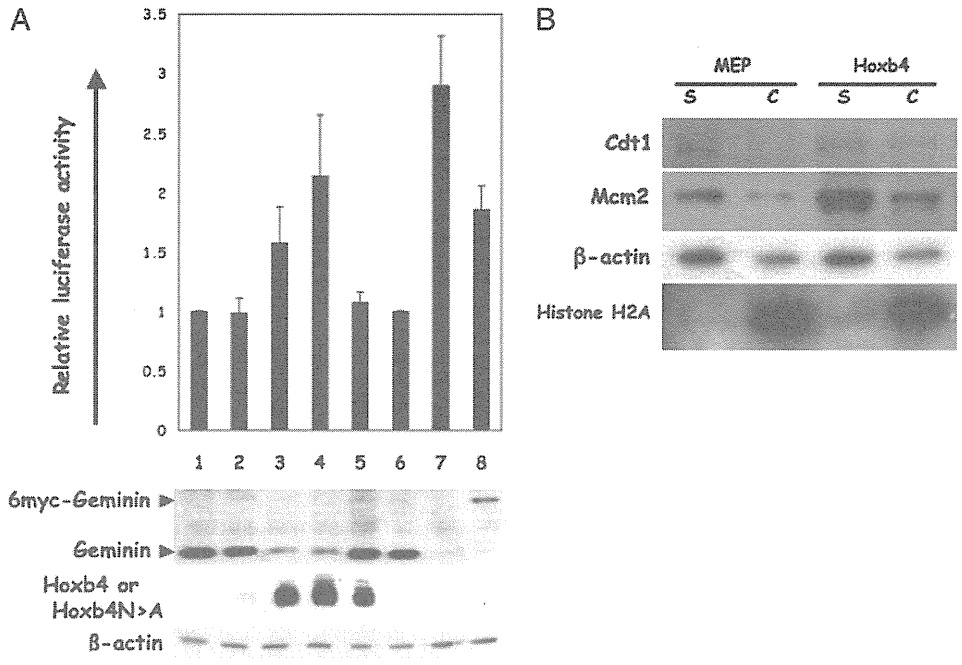

Fig. 6. Effect of Hoxb4 on E2F activity and DNA replication licensing. (*A*) Effect of Hoxb4 transfection on E2F activity. Renilla luciferase reporter plasmid driven by the mutant E2F-binding site, pE2MTx4-R, was used as control. (*Upper*) Firefly luciferase activity relative to that in mock vector-transfected cells. 1, mock vector; 2, Hoxb4—0.1 μg; 3, Hoxb4—0.5 μg; 4, Hoxb4—1 μg; 5, Hoxb4N>A—1 μg; 6, control siRNA; 7, siRNA for Geminin and a mock vector; 8, siRNA for Geminin and 6myc-tagged Geminin (0.1 μg). (*Lower*) Immunoblot analysis. (*B*) Effect of Hoxb4 transduction on Cdt1 and Mcm2 in the chromatin fraction of $Rae^{-/-}$FLC. S, soluble fraction; C, chromatin fraction. β-Actin and histone H2A were detected as control to ensure equal amounts of protein and purity of the chromatin fraction, respectively.

genetic evidence that the self-renewal and repopulating capacities, as well as hematopoietic differentiation, were impaired by *Cul4a* haploinsufficiency (24), although many target molecules for the Roc1-Ddb1-Cul4a component were reported. Hoxb4 transduction may down-regulate Geminin protein through UPS to relieve the inhibition of Cdt1, and down-regulated Geminin protein may also give rise to E2F activation, which facilitates loading of a DNA prereplicative complex onto chromatin to promote cell cycling. Because E2F activity was reported to be induced by Hoxb4 through the induction of c-Myc as mentioned above (9), Hoxb4 might induce E2F activity through either down-regulation of Geminin or up-regulation of c-Myc. Although it remains elusive in our study how down-regulated Geminin induces the E2F activation, the above findings suggest that Geminin by itself negatively regulates the transcription activity of its own promoter because transcription of *Geminin* is under the regulation of E2F (29). This may imply that a feedback mechanism plays a role in maintaining homeostasis of Geminin expression in cells. Hoxb4 transduction may thus affect Geminin homeostasis directly and indirectly, i.e., via the ubiquitination of Geminin and also via its effect on the transcription of *Geminin* to induce the HSC activity.

Although further detailed analysis is required, we propose a tentative model for the molecular mechanism showing how transduced Hoxb4 provides hematopoietic stem and progenitor cells with high proliferation potential on the basis of the findings in our current study (Fig. 7). Transduced Hoxb4 induces UPS-mediated down-regulation of Geminin protein by constituting the RDCOXB4 complex, an E3 ubiquitin ligase for Geminin, which results in augmentation of a prereplicative complex loaded onto chromatin as well as in transcription induction of the E2F target genes involved in DNA replication and cell cycling. The augmented prereplicative complex loaded onto chromatin may provide higher proliferation potential for hematopoietic stem and progenitor cells. As we previously reported, Geminin is highly expressed in $CD34^{-}KSL$ but is down-regulated in $CD34^{+}KSL$, progenitors, and their progeny subpopulations, whereas Cdt1 expression is reciprocal to Geminin expression (20). Thus, high Geminin expression is presumed to induce $CD34^{-}KSL$ to maintain quiescence and undifferentiated states through direct interaction with Cdt1(19) and Brg1/Brahma (21), respectively, whereas down-regulated Geminin may induce cellular proliferation and differentiation in the progeny subpopulations. Although the higher cellular proliferation potential might also help to induce self-renewal of HSCs, the precise molecular role for Geminin in Hoxb4 transduction-induced self-renewal activation of HSCs remains in-

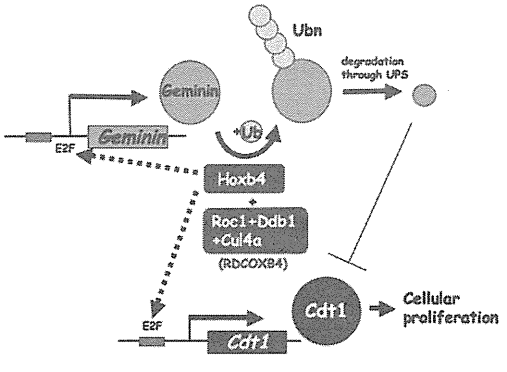

Fig. 7. Proposed tentative model for the molecular role of Hoxb4 in providing cells with proliferation potential. The pathway either enhanced or diminished by Hoxb4 transduction is indicated by thick and thin lines, respectively. Dotted lines indicated an indirect effect. E2F, E2F-binding site; Ub, ubiquitin.

sufficiently understood. Further detailed analysis of Geminin could provide an important clue for elucidating a molecular mechanism that sustains the hematopoietic stem and progenitor cell activity.

Materials and Methods

Animal experiments were done with C57BL6 mice and mice deficient in *Rae28* with a congenic genetic background. Plasmids and double-stranded RNAs (Dharmacon-ThermoFisher) were transfected by the calcium phosphate coprecipitation method and by using Lipofectamine RNAiMAX (Invitrogen-Life Technologies). Retrovirus-mediated gene transduction was performed with murine stem cell virus vectors. Hematopoiesis was assessed through clonogenic, LTC-IC, and LTR activities. The recombinant RDCOXB4 complexes were purified from Sf9 transfected with the baculovirus vectors and subjected to the in vitro ubiquitination assay. The statistically analyzed results are shown with SEM. A detailed description of all of the methods and antibodies used appear in *SI Materials and Methods* and in Table S1, respectively.

ACKNOWLEDGMENTS. We thank Drs. R. K. Humphries (University of British Columbia, Vancouver) and M. Kyba (University of Minnesota, Minneapolis) for providing the Hoxb4 cDNA; Dr. A. Kikuchi (Osaka University, Suita) for providing the pV-IKS and pVL1392 vectors; Dr. T. Inaba (Hiroshima University, Hiroshima) for the 32D cell line; the Analysis Center of Life Science in Hiroshima University, Ms. R. Tokimoto, and Y. Nakashima for technical assistance; Dr. M. Kanno (Hiroshima University, Hiroshima) for supporting Y.O., and Ms. A. Harada and H. Shimamoto for secretarial assistance. This work was supported by Grants-in-Aid for Scientific Research from the Ministry of Education, Culture, Sports, Science and Technology of Japan and by the Uehara Memorial Foundation, the Yamanouchi Foundation for Research on Metabolic Disorders, the Japan Leukaemia Research Fund, the Mitsubishi Pharma Research Foundation, the Novartis Foundation for the Promotion of Science, the Daiwa Securities Health Foundation, and the UBE Foundation.

1. Sauvageau G, et al. (1995) Overexpression of *HOXB4* in hematopoietic cells causes the selective expansion of more primitive populations in vitro and in vivo. *Genes Dev* 9: 1753–1765.
2. Antonchuk J, Sauvageau G, Humphries RK (2002) HOXB4-induced expansion of adult hematopoietic stem cells ex vivo. *Cell* 109:39–45.
3. Buske C, et al. (2002) Deregulated expression of HOXB4 enhances the primitive growth activity of human hematopoietic cells. *Blood* 100:862–868.
4. Kyba M, Perlingeiro RC, Daley GQ (2002) HoxB4 confers definitive lymphoid-myeloid engraftment potential on embryonic stem cell and yolk sac hematopoietic progenitors. *Cell* 109:29–37.
5. Amsellem S, et al. (2003) Ex vivo expansion of human hematopoietic stem cells by direct delivery of the HOXB4 homeoprotein. *Nat Med* 9:1423–1427.
6. Krosl J, et al. (2003) In vitro expansion of hematopoietic stem cells by recombinant TAT-HOXB4 protein. *Nat Med* 9:1428–1432.
7. McGinnis W, Krumlauf R (1992) Homeobox genes and axial patterning. *Cell* 68: 283–302.
8. Beslu N, et al. (2004) Molecular interactions involved in HOXB4-induced activation of HSC self-renewal. *Blood* 104:2307–2314.
9. Satoh Y, et al. (2004) Roles for c-Myc in self-renewal of hematopoietic stem cells. *J Biol Chem* 279:24986–24993.
10. Schiedlmeier B, et al. (2007) HOXB4's road map to stem cell expansion. *Proc Natl Acad Sci USA* 104:16952–16957.
11. Ohta H, et al. (2002) Polycomb group gene rae28 is required for sustaining activity of hematopoietic stem cells. *J Exp Med* 195:759–770.
12. Park IK, et al. (2003) Bmi-1 is required for maintenance of adult self-renewing haematopoietic stem cells. *Nature* 423:302–305.
13. Wang H, et al. (2004) Role of histone H2A ubiquitination in Polycomb silencing. *Nature* 431:873–878.
14. Takihara Y, et al. (1997) Targeted disruption of the mouse homologue of the *Drosophila polyhomeotic* gene leads to altered anteroposterior patterning and neural crest defects. *Development* 124:3673–3682.
15. Bracken AP, et al. (2007) The Polycomb group proteins bind throughout the INK4A-ARF locus and are disassociated in senescent cells. *Genes Dev* 21:525–530.
16. Chagraoui J, et al. (2006) E4F1: A novel candidate factor for mediating BMI1 function in primitive hematopoietic cells. *Genes Dev* 20:2110–2120.
17. Pomerantz J, et al. (1998) The Ink4a tumor suppressor gene product, p19Arf, interacts with MDM2 and neutralizes MDM2's inhibition of p53. *Cell* 92:713–723.
18. Le Cam L, et al. (2006) E4F1 is an atypical ubiquitin ligase that modulates p53 effector functions independently of degradation. *Cell* 127:775–788.
19. Blow JJ, Hodgson B (2002) Replication licensing: Defining the proliferative state? *Trends Cell Biol* 12:72–78.
20. Ohtsubo M, et al. (2008) Polycomb-group complex 1 acts as an E3 ubiquitin ligase for Geminin to sustain hematopoietic stem cell activity. *Proc Natl Acad Sci USA* 105: 10396–10401.
21. Seo S, et al. (2005) Geminin regulates neuronal differentiation by antagonizing Brg1 activity. *Genes Dev* 19:1723–1734.
22. Luo L, Yang X, Takihara Y, Knoetgen H, Kessel M (2004) The cell-cycle regulator geminin inhibits Hox function through direct and polycomb-mediated interactions. *Nature* 427:749–753.
23. Kim MY, et al. (2006) A repressor complex, AP4 transcription factor and geminin, negatively regulates expression of target genes in nonneuronal cells. *Proc Natl Acad Sci USA* 103:13074–13079.
24. Li B, et al. (2007) Cul4A is required for hematopoietic stem-cell engraftment and self-renewal. *Blood* 110:2704–2707.
25. Zhang Y, et al. (2003) CUL-4A stimulates ubiquitylation and degradation of the HOXA9 homeodomain protein. *EMBO J* 22:6057–6067.
26. McGarry TJ, Kirschner MW (1998) Geminin, an inhibitor of DNA replication, is degraded during mitosis. *Cell* 93:1043–1053.
27. Ohta T, Michel JJ, Schottelius AJ, Xiong Y (1999) ROC1, a homolog of APC11, represents a family of cullin partners with an associated ubiquitin ligase activity. *Mol Cell* 3:535–541.
28. Schulze A, et al. (1995) Cell cycle regulation of the cyclin A gene promoter is mediated by a variant E2F site. *Proc Natl Acad Sci USA* 92:11264–11268.
29. Yoshida K, Inoue I (2004) Regulation of Geminin and Cdt1 expression by E2F transcription factors. *Oncogene* 23:3802–3812.
30. Ohtani K, et al. (2000) Cell type-specific E2F activation and cell cycle progression induced by the oncogene product Tax of human T-cell leukemia virus type I. *J Biol Chem* 275:11154–11163.

Rapid Emergence of Telaprevir Resistant Hepatitis C Virus Strain from Wildtype Clone *In Vivo*

Nobuhiko Hiraga,[1,2] Michio Imamura,[1,2] Hiromi Abe,[1,2] C. Nelson Hayes,[1,2] Tomohiko Kono,[1,2] Mayu Onishi,[1,2] Masataka Tsuge,[1,2] Shoichi Takahashi,[1,2] Hidenori Ochi,[2,3] Eiji Iwao,[4] Naohiro Kamiya,[4] Ichimaro Yamada,[4] Chise Tateno,[2,5] Katsutoshi Yoshizato,[2,5] Hirotaka Matsui,[6] Akinori Kanai,[7] Toshiya Inaba,[6] Shinji Tanaka,[1,2] and Kazuaki Chayama[1,2,3]

Telaprevir is a potent inhibitor of hepatitis C virus (HCV) NS3-4A protease. However, the emergence of drug-resistant strains during therapy is a serious problem, and the susceptibility of resistant strains to interferon (IFN), as well as the details of the emergence of mutant strains *in vivo*, is not known. We previously established an infectious model of HCV using human hepatocyte chimeric mice. Using this system we investigated the biological properties and mode of emergence of mutants by ultra-deep sequencing technology. Chimeric mice were injected with serum samples obtained from a patient who had developed viral breakthrough during telaprevir monotherapy with strong selection for resistance mutations (A156F [92.6%]). Mice infected with the resistant strain (A156F [99.9%]) developed only low-level viremia and the virus was successfully eliminated with interferon therapy. As observed in patients, telaprevir monotherapy in viremic mice resulted in breakthrough, with selection for mutations that confer resistance to telaprevir (e.g., a high frequency of V36A [52.2%]). Mice were injected intrahepatically with HCV genotype 1b clone KT-9 with or without an introduced resistance mutation, A156S, in the NS3 region, and treated with telaprevir. Mice infected with the A156S strain developed lower-level viremia compared to the wildtype strain but showed strong resistance to telaprevir treatment. Although mice injected with wildtype HCV showed a rapid decline in viremia at the beginning of therapy, a high frequency (11%) of telaprevir-resistant NS3 V36A variants emerged 2 weeks after the start of treatment. *Conclusion:* Using deep sequencing technology and a genetically engineered HCV infection system, we showed that the rapid emergence of telaprevir-resistant HCV was induced by mutation from the wildtype strain of HCV *in vivo*. (HEPATOLOGY 2011;54:781-788)

Chronic hepatitis C virus (HCV) infection is a leading cause of cirrhosis, liver failure, and hepatocellular carcinoma.[1,2] The current standard treatment for patients chronically infected with HCV is the combination of peg-interferon (PEG-IFN) and ribavirin (RBV).[3-5] However, this treatment results in sustained viral response (SVR), defined as negative for HCV RNA 24 weeks after cessation of the therapy, in only about 50% of patients with genotype 1 HCV infection with high viral loads.[3-5] Given the low

Abbreviations: HCV, hepatitis C virus; HSA, human serum albumin; PEG-IFN, peg-interferon; RBV, ribavirin; RT-PCR, reverse transcript-polymerase chain reaction; SCID, severe combined immunodeficiency; SVR, sustained viral response; uPA, urokinase-type plasminogen activator.

From the [1]Department of Medicine and Molecular Science, Division of Frontier Medical Science, Programs for Biomedical Research, Graduate School of Biomedical Sciences, Hiroshima University, Hiroshima, Japan; [2]Liver Research Project Center, Hiroshima University, Hiroshima, Japan; [3]Laboratory for Digestive Diseases, RIKEN Center for Genomic Medicine, Hiroshima, Japan; [4]Research and Development Unit, Mitsubishi Tanabe Pharma Corp., Yokohama, Japan; [5]PhoenixBio Co., Ltd., Higashihiroshima, Japan; [6]Department of Molecular Oncology and Leukemia Program Project, Research Institute for Radiation Biology and Medicine, Hiroshima University, Hiroshima, Japan; [7]Radiation Research Center for Frontier Science, Research Institute for Radiation Biology and Medicine, Hiroshima University, Hiroshima, Japan.

Received January 17, 2011; accepted May 16, 2011.

Supported in part by a grant-in-aid for Scientific Research from the Japanese Ministry of Labor, Health and Welfare

Address reprint requests to: Prof. Kazuaki Chayama, M.D., Ph.D., Department of Medical and Molecular Science, Division of Frontier Medical Science, Programs for Biomedical Research, Graduate School of Biomedical Science, Hiroshima University, 1-2-3 Kasumi, Minami-ku, Hiroshima 734-8551, Japan. E-mail: chayama@hiroshima-u.ac.jp; fax: +81-82-255-6220.

View this article online at wileyonlinelibrary.com.

DOI 10.1002/hep.24460

Potential conflict of interest: E.I., N.K., I.Y. are employees of Mitsubishi Tanabe Pharma Corp. The other authors have nothing to declare.

effectiveness of the current therapy, many molecules have been screened for antiviral activity against HCV for use in development of novel anti-HCV therapies. A number of new selective inhibitors of HCV proteins, the so-called STAT-C (specifically targeted antiviral therapy for HCV) inhibitors, are currently under development. Telaprevir is a reversible, selective, specific inhibitor of the HCV NS3-4A protease that has shown potent antiviral activity in HCV replicon assays.[6] Although the antiviral effect of telaprevir is quite potent, monotherapy using these drugs results in rapid emergence of drug-resistant strains.[7,8] Accordingly, these drugs are used in combination with pegylated-IFN and ribavirin for chronic hepatitis C patients. Because the HCV virus replicates rapidly and RNA polymerase lacks a proofreading system, HCV viral quasispecies can emerge *de novo*, and some of these variants may confer resistance. Although a resistant variant is initially present at low frequency, it may quickly emerge as the dominant species during antiviral treatment.[9,10] Resistant clones against HCV NS3-4A protease inhibitors have reportedly been induced in replicon systems.

The immunodeficient urokinase-type plasminogen activator (uPA) mouse permits repopulation of the liver with human hepatocytes, resulting in human hepatocyte chimeric mice that are able to develop HCV viremia after injection of serum samples positive for the virus.[11] We and other groups have reported that the human hepatocyte chimeric mouse is useful for evaluating the effect of NS3-4A protease inhibitor.[12,13] Using this mouse model, we developed a reverse genetics systems for HCV.[14,15] This system is useful to study characteristics of HCV strains with various substitutions of interest because the confounding effects of quasispecies can be minimized. Using ultra-deep sequencing technology, we demonstrate the rapid emergence of telaprevir resistance in HCV as a result of mutation from wildtype strain using genetically engineered HCV-infected human hepatocyte chimeric mice.

Materials and Methods

Animal Treatment. Generation of the uPA$^{+/+}$/SCID$^{+/+}$ mice and transplantation of human hepatocytes were performed as described recently by our group.[16] All mice were transplanted with frozen human hepatocytes obtained from the same donor. Mice received humane care and all animal protocols were performed in accordance with the guidelines of the local committee for animal experiments. Infection, extraction of serum samples, and sacrifice were performed under ether anesthesia. Mice were injected either intravenously with HCV-positive human serum samples or intrahepatically with *in vitro*-transcribed genotype 1b HCV RNA. HCV-infected mice were administered either perorally with 200-300 mg/kg of telaprevir (VX950; MP424; Mitsubishi Tanabe Pharma, Osaka, Japan) twice a day or intramuscularly with 1,500 IU/g of IFN-alpha (Dainippon Sumitomo Pharma, Tokyo). The telaprevir dose was determined in a previous study in which this dosage range was found to yield serum concentrations equivalent to treated human patients.[13]

Human Serum Samples. After obtaining written informed consent, human serum samples containing genotype 1b HCV were obtained from two patients with chronic hepatitis. The individual serum samples were divided into aliquots and stored separately in liquid nitrogen until use. The study protocol conforms to the ethical guidelines of the 1975 Declaration of Helsinki and was approved *a priori* by the Institutional Review Committee.

HCV RNA Transcription and Inoculation into Chimeric Mice. We have previously established an infectious genotype 1b HCV clone HCV-KT9 derived from a Japanese patient with severe acute hepatitis (GenBank access. no. AB435162).[15] We cloned this HCV complementary DNA (cDNA) into plasmid pBR322 under a T7 RNA promoter to create the plasmid pHCV-KT9. Ten μg of plasmid DNA, linearized by *Xba*I (Promega, Madison, WI) digestion, were transcribed in a 100 μL reaction volume with T7 RNA polymerase (Promega) at 37°C for 2 hours and analyzed by agarose gel electrophoresis. Each transcription mixture was diluted with 400 μL of phosphate-buffered saline (PBS) and injected into the livers of chimeric mice.[15] The QuikChange site-directed mutagenesis kit (Stratagene, Foster City, CA) was used to introduce a substitution at amino acid 156 of the NS3 region (A156S).

RNA Extraction and Amplification. RNA was extracted from serum samples by Sepa Gene RV-R (Sankojunyaku, Tokyo), dissolved in 8.8 μL RNase-free H_2O, and reverse transcribed using a random primer (Takara Bio, Shiga, Japan) and M-MLV reverse transcriptase (ReverTra Ace, Toyobo, Osaka, Japan) in a 20-μL reaction mixture according to the instructions provided by the manufacturer. Nested polymerase chain reaction (PCR) and quantitation of HCV by Light Cycler (Roche Diagnostic, Japan, Tokyo) were performed as reported.[15]

Ultra-Deep Sequencing. We adapted multiplex sequencing-by-synthesis to simultaneously sequence

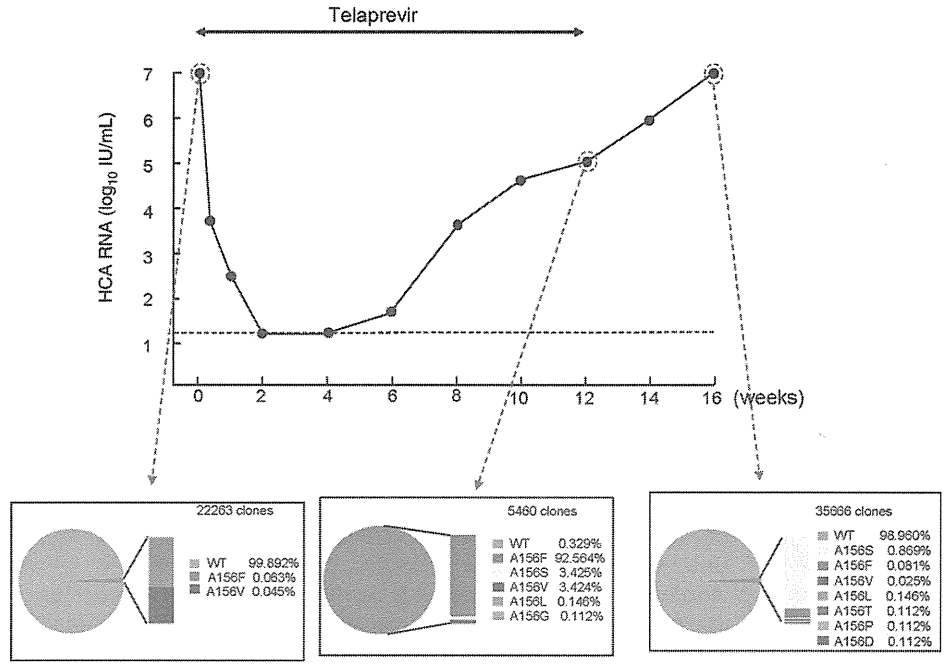

Fig. 1. Changes in serum HCV RNA levels in a telaprevir-treated chronic hepatitis C patient. A 55-year-old woman infected with genotype 1b HCV was treated with 750 mg of telaprevir every 8 hours for 12 weeks. Serum HCV RNA (upper panel) and the amino acid (aa) frequencies at aa156 in the HCV NS3 region by ultra-deep sequencing at the indicated times are shown. The horizontal dotted line indicates the detectable limit (1.2 log copy/mL).

multiple genomes using the Illumina Genome Analyzer. Briefly, cDNA was fragmented using sonication and the resultant fragment distribution was assessed using the Agilent BioAnalyzer 2100 platform. A library was prepared using the Multiplexing Sample Preparation Kit (Illumina, CA). Imaging analysis and base calling were performed using Illumina Pipeline software with default settings.[17-23] The N-terminal 543 nucleotides of NS3 protease were analyzed. This technique revealed an average coverage depth of over 1,000 sequence reads per basepair in the unique regions of the genome. Read mapping to a reference sequence was performed using Bowtie.[24] Because of the short 36 nucleotide read length, mapping hypervariable regions with multiple closely spaced variants against a reference sequence yields poor coverage. Therefore, common variants were identified by relaxing the mismatch settings as well as using *de novo* assembly using ABySS.[25] Multiple alternative reference sequences were included to improve coverage in variable regions. Codon counts were merged and analyzed using R v. 2.12.

Results

Emergence of a Telaprevir-Resistant Variant in a Hepatitis C Patient Treated with Telaprevir and Analysis of the A156F Mutation. A 55-year-old woman infected with genotype 1b HCV was treated with 750 mg of telaprevir every 8 hours for 12 weeks (Fig. 1). After 1 weeks of treatment, serum HCV RNA titer decreased below the detectable limit (1.2 log copy/mL). However, HCV RNA titer became positive by week 4. By week 12, HCV RNA titer had increased to 4.8 log copy/mL and telaprevir treatment was discontinued. Because direct sequence analysis showed an A156F mutation in the NS3 region in the serum samples at 12 weeks, we performed ultra-deep sequence analysis and confirmed the high frequency (92.5%) of A156F mutation. Four weeks after cessation of treatment (at 16 weeks), sequence analysis revealed that the major strain had reverted to wildtype (99%). To analyze the replication ability and the susceptibility of the A156F mutation to telaprevir, 100 μL serum samples containing 10^4 copies of HCV obtained at week 12 were injected into human hepatocyte chimeric mice. Two wildtype HCV-inoculated mice became positive for HCV RNA 2 weeks after inoculation and serum HCV RNA titer increased to high levels (7.6 and 7.8 log copy/mL, respectively) at 6 weeks after inoculation (Fig. 2). In contrast to wildtype HCV-infected mice, a mouse inoculated with serum containing the A156F mutant developed measurable viremia at 4 weeks postinoculation, although serum HCV RNA titer remained low at 6 weeks (5.2 log copy/mL). Eight weeks after inoculation ultra-deep sequence analysis showed a high frequency (99.9%) of A156F mutation. From this point the mouse was administrated 200 mg/kg of telaprevir perorally twice a day for 4 weeks. However, this treatment resulted in no reduction in serum HCV RNA level. During the observation period the A156F mutation remained at

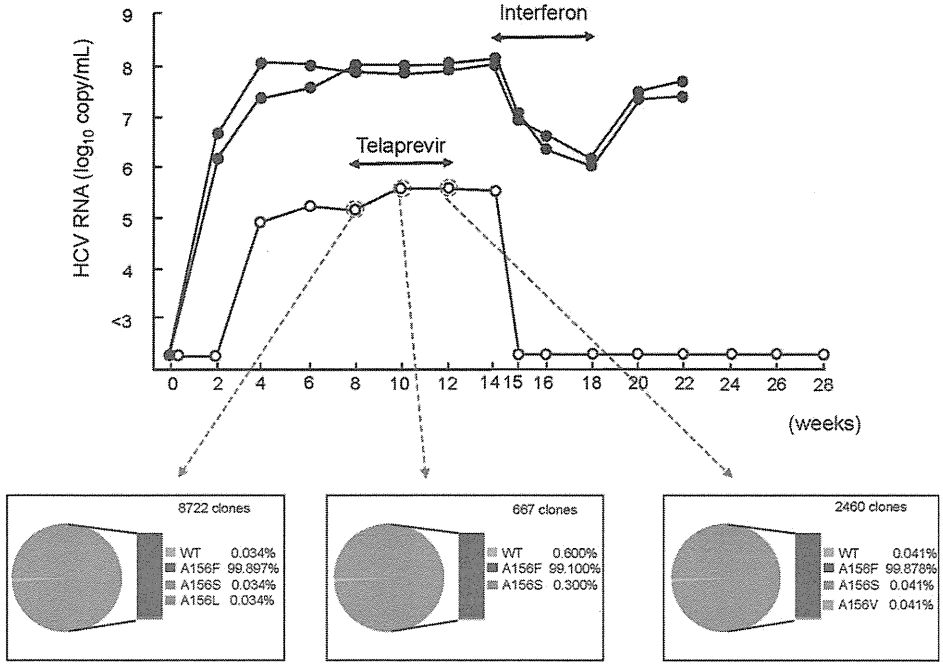

Fig. 2. Changes in serum virus titers in HCV-infected mice. Mice were injected with either wildtype (closed circles) or A156F-mutated HCV serum samples (obtained from an HCV-infected patient who received telaprevir monotherapy for 12 weeks; see Fig. 1) (open circles). Six weeks after injection the A156F mutant mouse was treated with 200 mg/kg of telaprevir orally twice a day for 4 weeks and injected intramuscularly with 1,500 IU/g/day of interferon-alpha for 4 weeks. Serum HCV RNA (upper panel) and amino acid (aa) frequencies at aa156 in the HCV NS3 region by ultra-deep sequencing at the indicated times are shown.

high frequency (>99%). To analyze the susceptibility of the A156F mutation to IFN, wildtype or A156F-mutated HCV-infected mice were treated with 1,500 IU/g/day of IFN-alpha for 4 weeks. Treatment resulted in only a two log reduction in HCV RNA level in wildtype HCV-infected mice. In contrast, serum HCV RNA titer decreased below the detectable limit 1 week after treatment in an A156F-infected mouse. Ten weeks after cessation of IFN-treatment (at week 28), HCV RNA in the mouse serum remained undetectable, suggesting that HCV RNA was eliminated. These results demonstrate that the A156F variant is associated with telaprevir-resistance, but the mutant has low replication ability and a high susceptibility to IFN.

Effect of Telaprevir on HCV-Infected Mice and Sequence Analysis of NS3 Region. Next we investigated the effect of telaprevir on wildtype HCV-infected mice. Two chimeric mice were inoculated intravenously with serum samples containing 10^5 copies of HCV obtained from an HCV-positive patient (Fig. 3). Six weeks after inoculation both mice were administered 200 mg/kg of telaprevir perorally twice a day for 4 weeks. Serum HCV RNA titer in both mice rapidly decreased; however, in one of the mice HCV RNA titer increased again 3 weeks after the start of treatment. Ultra-deep sequence analysis of the NS3 region showed that following the start of telaprevir administration the frequency of the V36A mutation increased from 18% at 2 weeks to 52% at 4 weeks, at which point it was accompanied by an increase in the HCV RNA titer. Two weeks after cessation of telaprevir treatment (at week 12), ultra-deep sequence analysis revealed that the frequency of the V36A mutant had decreased to 13% and the frequency of the wildtype HCV had increased to 84%, although the HCV RNA titer increased only slightly.

Intrahepatic Injection of HCV-KT9-Wild RNA and KT9-NS3-A156S RNA into Human Hepatocyte Chimeric Mice. We previously established an infectious genotype 1b HCV clone, HCV-KT9 (HCV-KT9-wild).[15] We created a telaprevir-resistant HCV clone by introducing an A156S amino acid substitution in the NS3 region of HCV-KT9 (KT9-NS3-A156S) (Fig. 4A). Using wildtype and telaprevir-resistant clones we investigated the replication ability *in vivo*. Mice were injected intrahepatically with 30 μg of *in vitro*-transcribed HCV-KT9-wild RNA or KT9-NS3-A156S RNA. Mice injected with HCV-KT9-wild developed measurable viremia at 2 weeks postinoculation and by 4 weeks postinoculation HCV RNA had reached 10^7 copy/mL (Fig. 4B). On the other hand, mice injected with KT9-NS3-A156S developed measurable viremia at 4 weeks postinoculation but maintained only low levels of viremia. These results suggest that the telaprevir-resistant HCV clone has a lowered replication ability compared to the wildtype HCV clone *in vivo*.

Treatment with Telaprevir and Analysis of Mutagenesis in Mice. Two mice infected with HCV-KT9-wild and one mouse infected with KT9-NS3-A156S were treated with 200 mg/kg of telaprevir twice a day for 2 weeks (Fig. 5A), resulting in 1.4 and 2.7 log

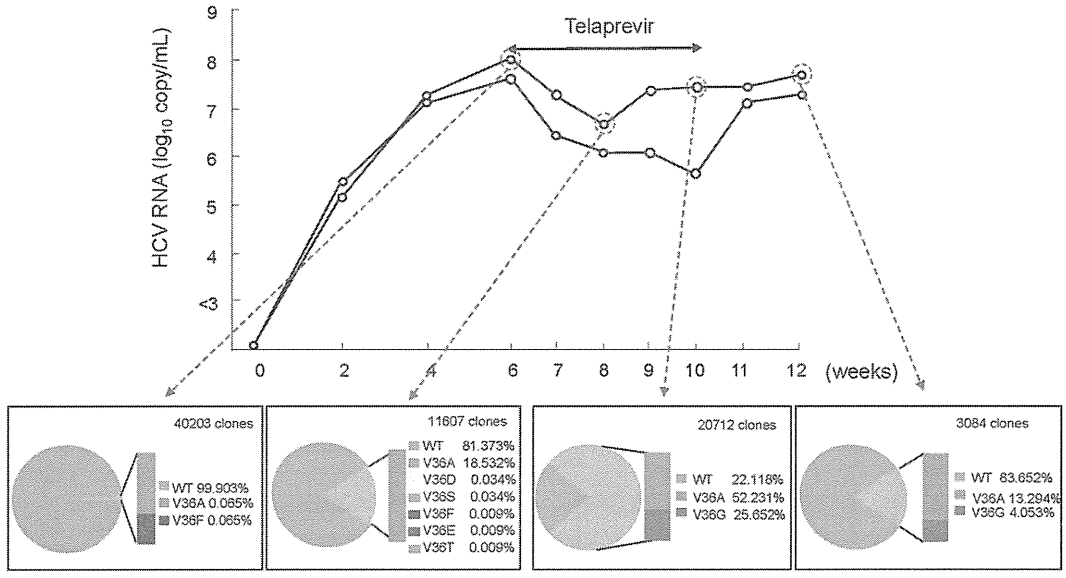

Fig. 3. Treatment with telaprevir in wildtype HCV-infected mice. Two mice were injected intravenously with 50 μL of HCV-positive human serum samples. Six weeks after HCV injection mice were treated with 200 mg/kg of telaprevir orally twice a day for 4 weeks. Serum HCV RNA (upper panel) and amino acid (aa) frequencies at aa36 in the HCV NS3 region by ultra-deep sequencing at the indicated times are shown.

reductions in HCV RNA level in the two wildtype HCV-infected mice. In contrast, only a 0.6 log reduction was observed in the KT9-NS3-A156S-infected mouse. These results demonstrate that our human hepatocyte chimeric mouse model infected with *in vitro*-transcribed HCV RNA provides an effective system for analysis of the susceptibility of HCV mutants to antiviral drugs. Interestingly, ultra-deep sequence analysis showed a rapid emergence of a V36A variant in the NS3 region in mouse serum 2 weeks after treatment (Fig. 5B). Four weeks after cessation of treatment (at week 6) the frequency of the V36A variant had decreased. Mice were then treated with 300 mg/kg of telaprevir twice a day for 4 weeks, which resulted in an elevated frequency of V36A variants at 1 (at week 7, 5.4%) and 4 weeks (at 10 week, 41.8%) after treatment and no reduction in serum HCV RNA level. These results suggest that telaprevir-resistant mutations emerged *de novo* from the wildtype strain of HCV, presumably through error-prone replication and potent selection for telaprevir escape mutants. During the telaprevir treatment period no increases of HCV RNA titers in these mice were observed, probably due to the low frequency of the resistant strain.

Discussion

Telaprevir is a peptidomimetic inhibitor of the NS3-4A serine protease that is currently undergoing clinical evaluation. Despite its effectiveness against HCV, some patients have shown a rapid viral breakthrough during the first 14 days of treatment.[26] Population sequencing of the viral NS3 region identified a number of mutations near the NS3 protease catalytic

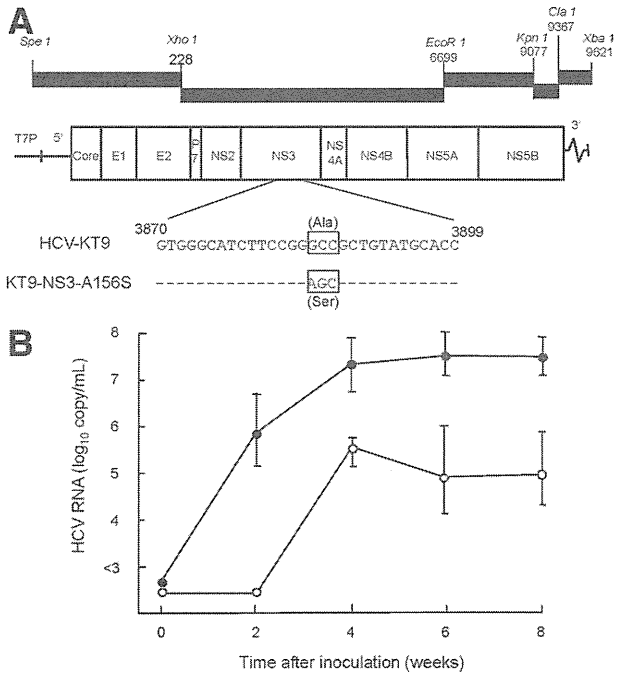

Fig. 4. Intrahepatic injection of *in vitro* transcribed HCV-KT9 RNA and KT9-NS3-A156S RNA into human hepatocyte chimeric mice. (A) The schematic of infectious genotype 1b HCV clones, HCV-KT9 and KT9-NS3-A156S. Boxes indicate codons at amino acid 156 in HCV NS3 region. Ala, alanine; Ser, serine. (B) Changes in serum levels of HCV RNA in mice intrahepatically injected with either HCV-KT9 RNA (closed circles) or KT9-NS3-A156S RNA (open circles). Data are represented as the mean ± SD of three mice.

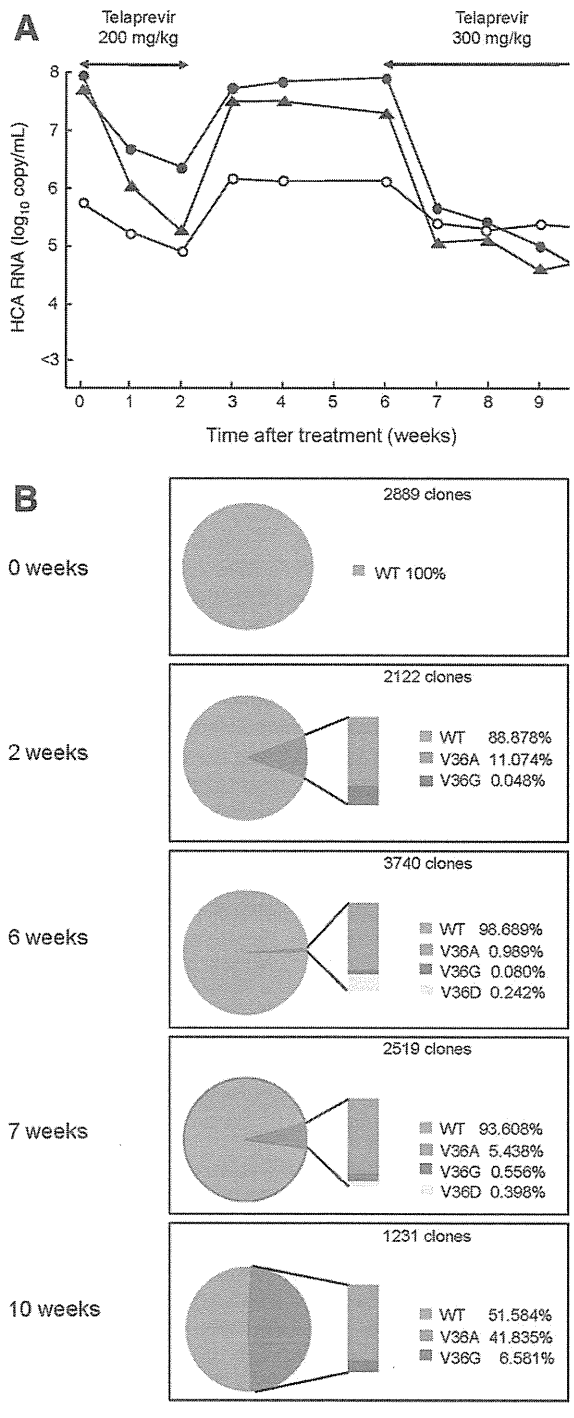

Fig. 5. The effect of telaprevir on mice infected with *in vitro*-transcribed HCV. Mice were injected with *in vitro*-transcribed HCV-KT9 RNA (closed circles and closed triangles) or KT9-NS3-A156S RNA (open circles). Six weeks after HCV RNA injection, mice were treated perorally with 200 mg/kg of telaprevir twice a day for 2 weeks. Four weeks after cessation of treatment mice were treated with 300 mg/kg of telaprevir twice a day for 4 weeks. (A) Mice serum HCV RNA titers at the indicated times are shown. Serum samples obtained from one of two HCV-KT9-infected mice (closed triangles) were used for ultra-deep sequencing. (B) Amino acid (aa) frequencies at aa36 in the HCV NS3 region based on ultra-deep sequencing are shown.

domain.[26] In particular, variants at NS3 residues 36, 54, 155, and 156 were shown to confer reduced sensitivity to telaprevir.[27]

In this study we analyzed the association between the antiviral efficacy of telaprevir and sequence variants within the NS3 region using chimeric mice infected with serum samples obtained from an HCV genotype 1b-infected patient. One of two HCV-infected mice had a viral breakthrough during the dosing period (Fig. 3). Ultra-deep sequence analysis of the NS3 region showed an increase of the V36A mutant, which has been reported to confer telaprevir resistance.[26] Consequently, our results show evidence of emergence of a telaprevir-resistant variant previously detected in human clinical trials.

We detected an A156F mutant in the HCV NS3 region in a chronic hepatitis patient who had experienced viral breakthrough during telaprevir monotherapy (Fig. 1). Likewise, HCV RNA titer in mice infected with the A156F variant showed no reduction following 2 weeks of telaprevir treatment (Fig. 2). However, 2 weeks of treatment with IFN-alpha rapidly suppressed serum HCV RNA titer below the detectable limit. These results demonstrate that A156F is telaprevir-resistant but has a high susceptibility to IFN.

Interestingly, ultra-deep sequencing revealed that the wildtype strain was present at low frequency (0.3%) in the serum inoculum (Fig. 2). However, the frequency of the wildtype failed to increase over time (Fig. 3), suggesting that the very small number of wildtype viral RNA (about 30 copies) may be incomplete or defective, as a large proportion of viral genomes are thought to be defective due to the virus's high replication and mutation rates.[9] Further analysis is necessary in order to interpret the significance of the presence of very low frequency variants detected by ultra-deep sequencing.

The short read lengths used in next generation sequencing also complicates the detection of rare variants, especially when variants are clustered within a region smaller than an individual read length (e.g., 36 basepairs). Relaxing the matching criteria allows mapping of more diverse reads but increases the error rate, whereas default settings may be geared toward more genetically homogenous haploid or diploid genomes. In this study we used *de novo* assembly to identify more diverse variants that failed to map to the reference sequence. Examining the variation in codon frequencies among samples, we created alternative reference sequences containing a sufficient range of variants to provide more uniform coverage of variable regions.

Using our previously established infectious HCV-KT9 genotype 1b HCV clone, we investigated the antiviral efficacy of telaprevir and the effect of

resistance mutations on viral replication. HCV RNA titer in mice infected with the telaprevir-resistant strain KT9-NS3-A156S was lower than in mice infected with the wildtype strain HCV-KT9-wild (Fig. 4B). HCV NS proteins include proteases for sequential processing of the polyprotein and are thought to be important in viral replication.[28] Our results suggest that differences in viral fitness underlie the differences in viral replication capacity. We analyzed the antiviral efficacy of telaprevir and the sequence of the NS3 region using HCV-infected mice treated with telaprevir. Although telaprevir treatment suppressed serum HCV RNA titer in mice infected with HCV-KT9, the decline of HCV RNA titer was only 0.6 log copy/mL in a mouse infected with KT9-NS3-A156S under the same treatment (Fig. 5A). These results suggest that our genetically engineered HCV-infected mouse model is useful for analyzing HCV escape mutants associated with antiviral drugs. Interestingly, treatment with telaprevir resulted in selection for V36A variants in the NS3 region in an HCV-KT9-infected mouse (Fig. 5B). There are a few controversial reports proposing that resistant variants may already be present at low frequency (<1%) within the quasispecies population in treatment-naïve patients,[29] consistent with their rapid emergence only days after treatment initiation.[26,30] This might well occur, due to the large number of mutated HCV clones. However, our results provide evidence in support of *de novo* emergence of telaprevir resistance induced by viral mutation followed by selection. HCV has both a high replication rate (10^{12} particles per day) and a high mutation rate (10^{-3} to 10^{-4}),[9,10] suggesting that the viral quasispecies population is likely to represent a large and genetically diverse substrate for immune selection.

In summary, we established an infection model of a genotype 1b HCV clone using the human hepatocyte chimeric mouse model. Using this model we demonstrate rapid emergence of *de novo* telaprevir-resistant HCV quasispecies from wildtype HCV.

Acknowledgment: The authors thank Rie Akiyama, Kazuyo Hattori, Yoshie Yoshida, Kiyomi Toyota, and Yoko Matsumoto for expert technical assistance.

References

1. Kiyosawa K, Sodeyama T, Tanaka E, Gibo Y, Yoshizawa K, Nakano Y, et al. Interrelationship of blood transfusion, non-A, non-B hepatitis and hepatocellular carcinoma: analysis by detection of antibody to hepatitis C virus. HEPATOLOGY 1990;12:671-675.
2. Niederau C, Lange S, Heintges T, Erhardt A, Buschkamp M, Hurter D, et al. Prognosis of chronic hepatitis C: results of a large, prospective cohort study. HEPATOLOGY 1998;28:1687-1695.
3. Manns MP, McHutchison JG, Gordon SC, Rustgi VK, Shiffman M, Reindollar R, et al. Peginterferon alfa-2b plus ribavirin compared with interferon alfa-2b plus ribavirin for initial treatment of chronic hepatitis C: a randomised trial. Lancet 2001;358:958-965.
4. Fried MW, Shiffman ML, Reddy KR, Smith C, Marinos G, Goncales FL Jr, et al. Peginterferon alfa-2a plus ribavirin for chronic hepatitis C virus infection. N Engl J Med 2002;347:975-982.
5. Hoofnagle JH, Ghany MG, Kleiner DE, Doo E, Heller T, Promrat K, et al. Maintenance therapy with ribavirin in patients with chronic hepatitis C who fail to respond to combination therapy with interferon alfa and ribavirin. HEPATOLOGY 2003;38:66-74.
6. Perni RB, Almquist SJ, Byrn RA, Chandorkar G, Chaturvedi PR, Courtney LF, et al. Preclinical profile of VX-950, a potent, selective, and orally bioavailable inhibitor of hepatitis C virus NS3–4A serine protease. Antimicrob Agents Chemother 2006;50:899-909.
7. Lin C, Gates CA, Rao BG, Brennan DL, Fulghum JR, Luong YP, et al. In vitro studies of cross-resistance mutations against two hepatitis C virus serine protease inhibitors, VX-950 and BILN 2061. J Biol Chem 2005;280:36784-36791.
8. Mo H, Lu L, Pilot-Matias T, Pithawalla R, Mondal R, Masse S, et al. Mutations conferring resistance to a hepatitis C virus (HCV) RNA-dependent RNA polymerase inhibitor alone or in combination with an HCV serine protease inhibitor in vitro. Antimicrob Agents Chemother 2005;49:4305-4314.
9. Bartenschlager R, Lohmann V. Replication of hepatitis C virus. J Gen Virol 2000;81:1631-1648.
10. Rong L, Dahari H, Ribeiro RM, Perelson AS. Rapid emergence of protease inhibitor resistance in hepatitis C virus. Sci Transl Med 2010;2:30ra32.
11. Mercer DF, Schiller DE, Elliott JF, Douglas DN, Hao C, Rinfret A, et al. Hepatitis C virus replication in mice with chimeric human livers. Nat Med 2001;7:927-933.
12. Kneteman NM, Weiner AJ, O'Connell J, Collett M, Gao T, Aukerman L, et al. Anti-HCV therapies in chimeric scid-Alb/uPA mice parallel outcomes in human clinical application. HEPATOLOGY 2006;43:1346-1353.
13. Kamiya N, Iwao E, Hiraga N, Tsuge M, Imamura M, Takahashi S, et al. Practical evaluation of a mouse with chimeric human liver model for hepatitis C virus infection using an NS3–4A protease inhibitor. J Gen Virol 2010;91:1668-1677.
14. Hiraga N, Imamura M, Tsuge M, Noguchi C, Takahashi S, Iwao E, et al. Infection of human hepatocyte chimeric mouse with genetically engineered hepatitis C virus and its susceptibility to interferon. FEBS Lett 2007;581:1983-1987.
15. Kimura T, Imamura M, Hiraga N, Hatakeyama T, Miki D, Noguchi C, et al. Establishment of an infectious genotype 1b hepatitis C virus clone in human hepatocyte chimeric mice. J Gen Virol 2008;89:2108-2113.
16. Tateno C, Yoshizane Y, Saito N, Kataoka M, Utoh R, Yamasaki C, et al. Near completely humanized liver in mice shows human-type metabolic responses to drugs. Am J Pathol 2004;165:901-912.
17. Cronn R, Liston A, Parks M, Gernandt DS, Shen R, Mockler T. Multiplex sequencing of plant chloroplast genomes using Solexa sequencing-by-synthesis technology. Nucleic Acids Res 2008;36:e122.
18. Mitsuya Y, Varghese V, Wang C, Liu TF, Holmes SP, Jayakumar P, et al. Minority human immunodeficiency virus type 1 variants in antiretroviral-naive persons with reverse transcriptase codon 215 revertant mutations. J Virol 2008;82:10747-10755.
19. Margeridon-Thermet S, Shulman NS, Ahmed A, Shahriar R, Liu T, Wang C, et al. Ultra-deep pyrosequencing of hepatitis B virus quasispecies from nucleoside and nucleotide reverse-transcriptase inhibitor (NRTI)-treated patients and NRTI-naive patients. J Infect Dis 2009;199:1275-1285.
20. Szpara ML, Parsons L, Enquist LW. Sequence variability in clinical and laboratory isolates of herpes simplex virus 1 reveals new mutations. J Virol 2010;84:5303-5313.

21. Wright CF, Morelli MJ, Thebaud G, Knowles NJ, Herzyk P, Paton DJ, et al. Beyond the consensus: dissecting within-host viral population diversity of foot-and-mouth disease virus by using next-generation genome sequencing. J Virol 2011;85:2266-2275.
22. Verbinnen T, Van Marck H, Vandenbroucke I, Vijgen L, Claes M, Lin TI, et al. Tracking the evolution of multiple in vitro hepatitis C virus replicon variants under protease inhibitor selection pressure by 454 deep sequencing. J Virol 2010;84:11124-11133.
23. Wang GP, Sherrill-Mix SA, Chang KM, Quince C, Bushman FD. Hepatitis C virus transmission bottlenecks analyzed by deep sequencing. J Virol 2010;84:6218-6228.
24. Langmead B, Trapnell C, Pop M, Salzberg SL. Ultrafast and memory-efficient alignment of short DNA sequences to the human genome. Genome Biol 2009;10:R25.
25. Simpson JT, Wong K, Jackman SD, Schein JE, Jones SJ, Birol I. ABySS: a parallel assembler for short read sequence data. Genome Res 2009;19:1117-1123.
26. Sarrazin C, Kieffer TL, Bartels D, Hanzelka B, Muh U, Welker M, et al. Dynamic hepatitis C virus genotypic and phenotypic changes in patients treated with the protease inhibitor telaprevir. Gastroenterology 2007;132:1767-1777.
27. Kuntzen T, Timm J, Berical A, Lennon N, Berlin AM, Young SK, et al. Naturally occurring dominant resistance mutations to hepatitis C virus protease and polymerase inhibitors in treatment-naive patients. HEPATOLOGY 2008;48:1769-1778.
28. Hijikata M, Mizushima H, Tanji Y, Komoda Y, Hirowatari Y, Akagi T, et al. Proteolytic processing and membrane association of putative nonstructural proteins of hepatitis C virus. Proc Natl Acad Sci U S A 1993;90:10773-10777.
29. Lu L, Mo H, Pilot-Matias TJ, Molla A. Evolution of resistant M414T mutants among hepatitis C virus replicon cells treated with polymerase inhibitor A-782759. Antimicrob Agents Chemother 2007;51:1889-1896.
30. Kieffer TL, Sarrazin C, Miller JS, Welker MW, Forestier N, Reesink HW, et al. Telaprevir and pegylated interferon-alpha-2a inhibit wild-type and resistant genotype 1 hepatitis C virus replication in patients. HEPATOLOGY 2007;46:631-639.

THE JOURNAL OF BIOLOGICAL CHEMISTRY VOL. 286, NO. 7, pp. 5589–5598, February 18, 2011

The Dynactin Complex Maintains the Integrity of Metaphasic Centrosomes to Ensure Transition to Anaphase*[S]

Received for publication, July 22, 2010, and in revised form, December 14, 2010 Published, JBC Papers in Press, December 16, 2010, DOI 10.1074/jbc.M110.167742

Yuko Ozaki, Hirotaka Matsui, Akiko Nagamachi, Hiroya Asou, Daisuke Aki, and Toshiya Inaba[1]

From the Department of Molecular Oncology and Leukemia Program Project, Research Institute for Radiation Biology and Medicine, Hiroshima University, Hiroshima 734-8553, Japan

The dynactin complex is required for activation of the dynein motor complex, which plays a critical role in various cell functions including mitosis. During metaphase, the dynein-dynactin complex removes spindle checkpoint proteins from kinetochores to facilitate the transition to anaphase. Three components ($p150^{Glued}$, dynamitin, and p24) compose a key portion of the dynactin complex, termed the projecting arm. To investigate the roles of the dynactin complex in mitosis, we used RNA interference to down-regulate p24 and $p150^{Glued}$ in human cells. In response to p24 down-regulation, we observed cells with delayed metaphase in which chromosomes frequently align abnormally to resemble a "figure eight," resulting in cell death. We attribute the figure eight chromosome alignment to impaired metaphasic centrosomes that lack spindle tension. Like p24, RNA interference of $p150^{Glued}$ also induces prometaphase and metaphase delays; however, most of these cells eventually enter anaphase and complete mitosis. Our findings suggest that although both p24 and $p150^{Glued}$ components of the dynactin complex contribute to mitotic progression, p24 also appears to play a role in metaphase centrosome integrity, helping to ensure the transition to anaphase.

The dynein-dynactin complex, a minus end-directed microtubule-based motor, carries out diverse transport activities indispensable for various cell functions and behaviors (Ref. 1 and references therein). For instance, the dynein-dynactin complex transports giant centrosomal scaffold proteins such as CG-NAP/AKAP450 and NuMA and induces smooth progression through mitosis. This motor complex also contributes to the transition from metaphase to anaphase: To ensure that each daughter cell receives only one chromosome set, the spindle assembly checkpoint blocks entry into anaphase until kinetochores on sister chromatids are attached to opposite spindle poles. Once this condition is achieved, the dynein-dynactin motor induces passage through the spindle checkpoint by removing critical checkpoint proteins (such as BubR1 or Mad2) from kinetochores.

* This work was supported by grants-in-aid for scientific research from the Ministry of Education, Culture, Sports, Science and Technology of Japan.
[S] The on-line version of this article (available at http://www.jbc.org) contains supplemental Movies 1–3.
[1] To whom correspondence should be addressed: 1-2-3 Kasumi, Minami-ku, Hiroshima 734-8553, Japan. Fax: 81-82-256-7103; E-mail: tinaba@hiroshima-u.ac.jp.

Dynactin is composed of 10 subunit proteins that are required for dynein activation (2) and references therein). Three proteins among them, $p150^{Glued}$ (dynactin 1), dynamitin (p50 and dynactin 2), and p24 (dynactin 3) (3, 4), constitute a flexible and extendable structure (the projecting arm) that associates directly with microtubules and the dynein complex.

Each dynactin molecule contains two copies of $p150^{Glued}$ and p24 and four copies of dynamitin. All three proteins are evolutionarily conserved from yeast to mammalian cells (5, 6), suggesting that these components are essential for the formation of a functional projecting arm. Within this substructure, $p150^{Glued}$ is sufficient for binding to dynein and for traversing the microtubule lattice, whereas dynamitin also plays a critical role in association with the dynein complex and in promotion of dynein-based movement. It is noteworthy that overexpression of dynamitin disrupts dynactin structure (7). Although the mechanism underlying this disruption is yet to be elucidated, dynamitin overexpression has been the major tool in molecular biology for down-regulation of dynactin function (2). Indeed, dynamitin overexpression was used to verify involvement of the dynactin complex in the spindle checkpoint silencing that induces metaphase arrest/delay (8).

In contrast to $p150^{Glued}$ or dynamitin, little is known about the role of the p24 subunit in mitosis. Although Ldb18 (a *Saccharomyces cerevisiae* homolog of p24) is essential for attachment of $p150^{Glued}$ to dynamitin and to the remainder of the dynactin complex (6), low amino acid identity between Ldb18 and human p24 (16.9%) does not favor speculation on the roles of mammalian p24.

RNAi is currently the most useful method for down-regulating the expression of a specific gene. Although several authors report successful suppression of $p150^{Glued}$ using siRNA or shRNA (8–10), their papers did not describe any mitotic abnormalities in cells expressing reduced levels of $p150^{Glued}$. Moreover, there have been no reports of p24 down-regulation using the RNAi method. In this report, we use RNAi to down-regulate p24 and $p150^{Glued}$ proteins in human cells. Our results demonstrate that cells expressing reduced levels of either p24 or $p150^{Glued}$ both show severe metaphase delay but that other mitotic disturbances differ between the two suppressed genes.

EXPERIMENTAL PROCEDURES

Cell Culture and Transfection of siRNA—HeLa, U2OS, and HEK 293 cell lines and their derivative cells were cultured in Dulbecco's modified Eagle's medium supplemented with 10% FBS. siRNA oligonucleotides for $p150^{Glued}$ (siRNA-p150, 5′-

GACTTCACCCCTTGATTAA-3′; siRNA-p150b, 5′-CCACCACCAAAGGUUAAGU-3′) (10) or p24 (siRNA-p24, 5′-CCGCATTGCCATACCTGAT-3; siRNA-p24b, 5′-GCUACUUUGCCAGCUAGAG-3′) were transfected at a concentration of 100 nM into HeLa(tc), a HeLa subline (11) or U2OS cells using Oligofectamine (Invitrogen), otherwise indicated in text and figure legends. Dead cells were identified using the trypan blue dye exclusion test. p24 and H2B-GFP were expressed using the pcDNA3 expression vector (Invitrogen).

Rescue Experiments—An siRNA-p24-resistant p24 cDNA was created by changing six nucleotides in the target sequence of siRNA-p24 that have no effect on amino acid sequence (CCGAATAGCAATCCCAGAC; underlined letters indicate replaced nucleotides). Because the target sequence for siRNA-p150 is in the 3′-UTR, we used a p150 cDNA 3′-UTR truncation (a gift of Dr. M. Katsuno and G. Sobue (12)) to generate a siRNA-p150-resistant p150 cDNA. To generate a pantropic retrovirus, HEK 293 cells were co-transfected with three plasmids: pHIT60 expressing murine leukemia virus gag pol (a gift of Dr. A. J. Kingsman (13)), pHCMV-G for vesicular stomatitis virus enveloped pseudotypes (a gift of Dr. T. Friedmann (14)), and pMSCV (Clontech) driving expression of siRNA-resistant p24 or p150 cDNA and IRES-EGFP[2] (15).

Analysis of mRNA and Protein Expression—Real-time quantitative RT-PCR was performed as described previously (16) using primer sets (p24 (forward, 5′-GAGTACATCGACCGCATTGCCATAC-3′ and reverse, 5′-TGATGTGAGCACTGTCCAGCATGG-3′) and p150^{Glued} (forward, 5′-TGCAGGCCACGCTACACCGCTATG-3′ and reverse, 5′-GCAATATCTGTAGCCTCCTGCCCAC-3′)). Immunostaining and image analyses were performed as described (11, 17). Signal specificity was tested by adding antigen for each antibody into the blocking solution. Relative fluorescence intensity was measured using ImageJ software. Immunoprecipitation and immunoblot analyses were performed according to standard procedures (18).

TUNEL—TUNEL assays were performed using the Fluorometric TUNEL assay kit (Promega, Madison, WI). Briefly, cells fixed with paraformaldehyde and ethanol were incubated with fluorescein-dUTP and terminal deoxynucleotidyl transferase for one hour at 37 °C. Cells were propidium iodide-stained immediately prior to flow cytometry analysis (FACSCalibur, BD Biosciences).

Fluorescence in Situ Hybridization (FISH)—HeLa cells cultured on coverglass slips were fixed with 3.7% formaldehyde, denatured on a heat block, and used directly for FISH analysis using a Myc probe complementary to chromosome band 8q24 (Dako, Glostrup, Denmark) according to the manufacturer's protocol.

Reagents—Rabbit anti-p24 polyclonal antibodies were raised against a GST-p24(N) (amino acids 5–36) or a GST-p24(C) polypeptide (amino acids 145–186) and then affinity purified according to standard procedures (18). Commercial antibodies were purchased from the following suppliers: p150^{Glued} from BD Biosciences; actin (product no. 1378 996) from Roche Diagnostics; and α-tubulin (product no. T9026) and γ-tubulin (product no. T6557) from Sigma. Hoechst 33342 was purchased from Invitrogen.

[2] The abbreviations used are: EGFP, enhanced GFP; FISH, fluorescence in situ hybridization; IRES, internal ribosomal entry site.

RESULTS

Down-regulation of p24 and p150^{Glued} Using siRNA—We initially used HeLa(tc) cells, a HeLa subline that allows high efficiency siRNA transfection (typically >90%) (11), for siRNA transfections. HeLa(tc) cells treated with siRNA (100 nM for 24 h) specific for p24 (siRNA-p24) or p150^{Glued} (siRNA-p150) showed a 5-fold approximate decrease in mRNA expression levels relative to cells treated with scrambled control siRNA (control siRNA) (Fig. 1*A*).

We used rabbits to generate two polyclonal antibodies, p24(N) and p24(C), against different portions of p24 (see "Experimental Procedures"). Both antibodies recognized an endogenous p24 protein (Fig. 1*B*, *lane 1*) that migrated to the same position in SDS-polyacrylamide gels as exogenous p24 protein expressed from a eukaryote plasmid expression vector (*lane 4*). As previously reported, the apparent mass of p24 is ~21 kDa, slightly smaller than the mass predicted from the amino acid sequence (4). Cells treated with siRNA-p24 (100 nM) for 48 h expressed 10-fold lower levels of p24 protein relative to untreated cells or cells treated with control siRNA (*lane 3*). Immunoblot analysis using p150^{Glued} antibody revealed a 20-fold reduction in p150^{Glued} protein levels in cells treated with siRNA-p150 for 72 h (Fig. 1*C*).

Similar to previous reports (4), immunostaining of mitotic cells with p24(C) antibody showed p24 localized to kinetochores and centrosomes in prometaphase and metaphase cells with considerable signal remaining in early anaphase (Fig. 1*D*). Although the general localization of p150^{Glued} (Fig. 1*E*) overlaps with p24, some specific differences were distinguished in cells doubly stained with p24 and p150^{Glued} antibodies (Fig. 1*F*). First, staining of mitotic spindles with anti-p150 was strong, whereas only weak fluorescence was detected with anti-p24. Second, although both p24 and p150 signals were detected at prometaphase kinetochores, p150 signal intensity diminished rapidly in metaphase, whereas p24 signals were remained until anaphase. The contrast between the intense p24 immunofluorescence maintained in anaphase centrosomes with diminished p150^{Glued} immunofluorescence that is barely detectable in early anaphase suggests a rapid efflux of p150^{Glued} from centrosomes during metaphase.

When cells were transfected with Cy3-labeled siRNA-p24, the intensity of p24 immunofluorescence in Cy3 staining-positive cells was reduced (Fig. 1*G*, *left panels*). p150^{Glued} signals were also reduced in response to treatment with siRNA-p150 (100 nM) for 72 h (*right panels*).

siRNA-p24 or -p150 Induces Mitotic Disturbances—Although we observed no obvious morphological differences in phase-contrast microscopy images of interphasic HeLa(tc) cells treated for up to 72 h with control siRNA, siRNA-p24, or siRNA-p150 (100 nM) (data not shown), we did observe a significant increase in the mitotic index of cells 48 h after transfection with siRNA-p24 relative to control siRNA (11.1% relative to 4%) ($p < 0.01$, Chi-square test, Fig. 2*A*). In addition,

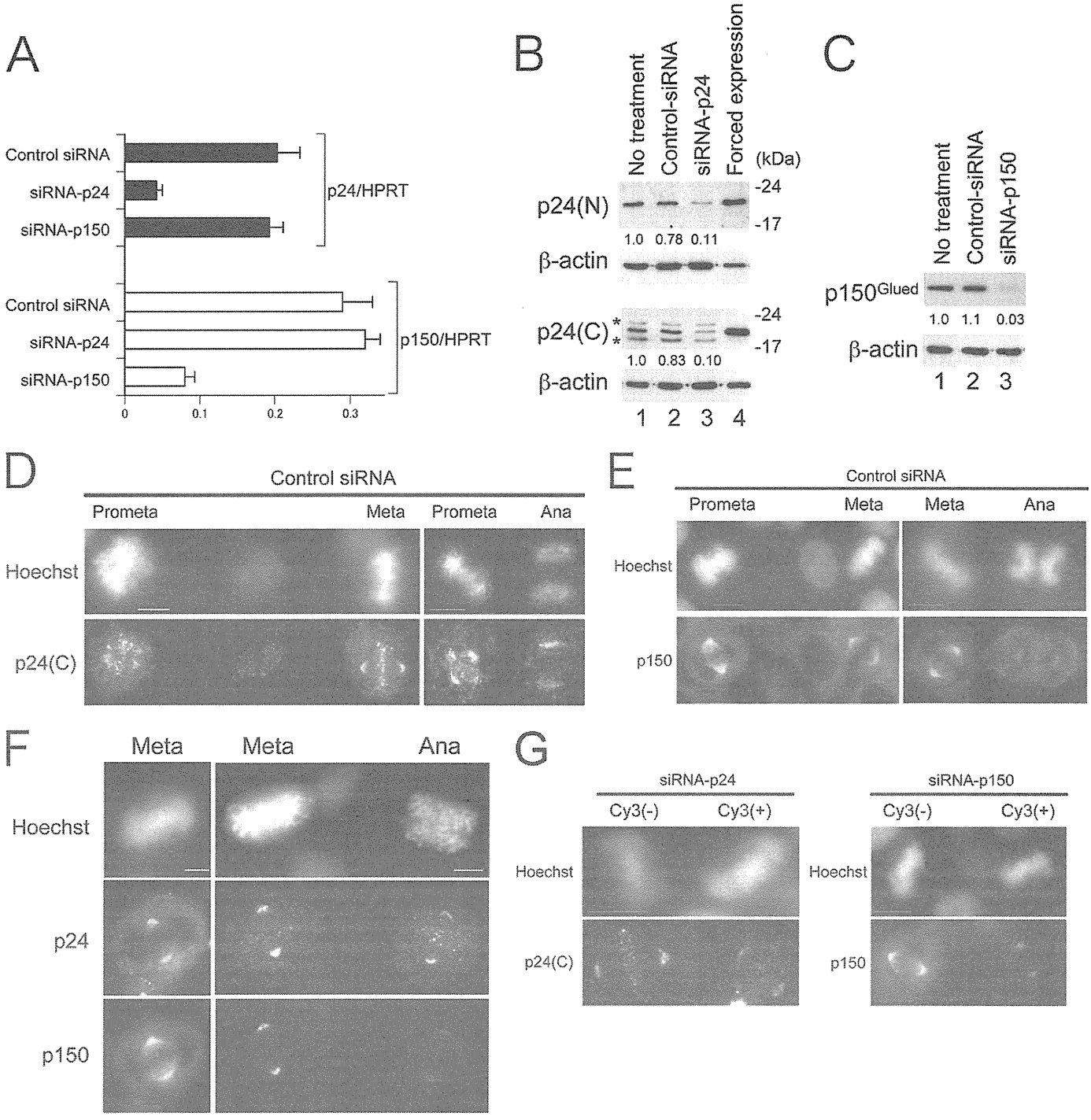

FIGURE 1. **Down-regulation of p24 and p150 by siRNA.** *A*, p24 (*black bars*) and p150^{Glued} (*open bars*) mRNA expression levels in HeLa(tc) cells treated with control siRNA, siRNA-p24, or siRNA-p150 (100 nM) for 24 h. Real-time quantitative PCR data were normalized against hypoxanthine phosphoribosyl transferase (*HPRT*), and the mean and S.D. for three independent experiments is represented. *B*, immunoblot analysis using p24(N), p24(C), or β-actin antibody. *Lane 1*, untreated HeLa(tc) cells; *lane 2*, cells treated with control siRNA (100 nM) for 48 h; *lane 3*, cells treated with siRNA-p24 (100 nM) for 48 h; *lane 4*, HEK 293 cells transfected with pcDNA3-p24, a eukaryotic expression vector. Ratios of relative intensity (p24/actin) measured by densitometry are indicated below each lane. *Asterisks* indicate cross-reactive bands appearing in HeLa but not HEK 293 cells. *C*, immunoblot analysis using p150^{Glued} or β-actin antibody. *Lane 1*, untreated HeLa(tc) cells; *lane 2*, cells treated with control siRNA (100 nM) for 72 h; *lane 3*, cells treated with siRNA-p150 (100 nM) for 72 h. Ratios of relative intensity (p150/actin) measured by densitometry are shown below. *D–G*, immunostaining of mitotic HeLa cells treated with siRNA indicated *above* with antibodies indicated on the *left*. DNA was stained with Hoechst 33342, and the mitotic phase of cells are labeled above. *Bars*, 10 μm (*D*, *E*, and *G*) and 5 μm (*F*). *Meta*, metaphase; *Ana*, anaphase; *Prometa*, prometaphase.

there was also a significant increase ($p < 0.01$) in the number of dead cells (determined by trypan blue dye exclusion) among the cells treated with siRNA-p24 for 48 and 72 h (7.2%, 15/207 and 17.1% 36/211, respectively) and siRNA-p150 for 72 h (8.0%, 16/202) relative to untreated cells (2.0%, 8/401).

Flow cytometric analyses of HeLa cells treated with siRNA-p24 for 48 h and stained with propidium iodide dem-

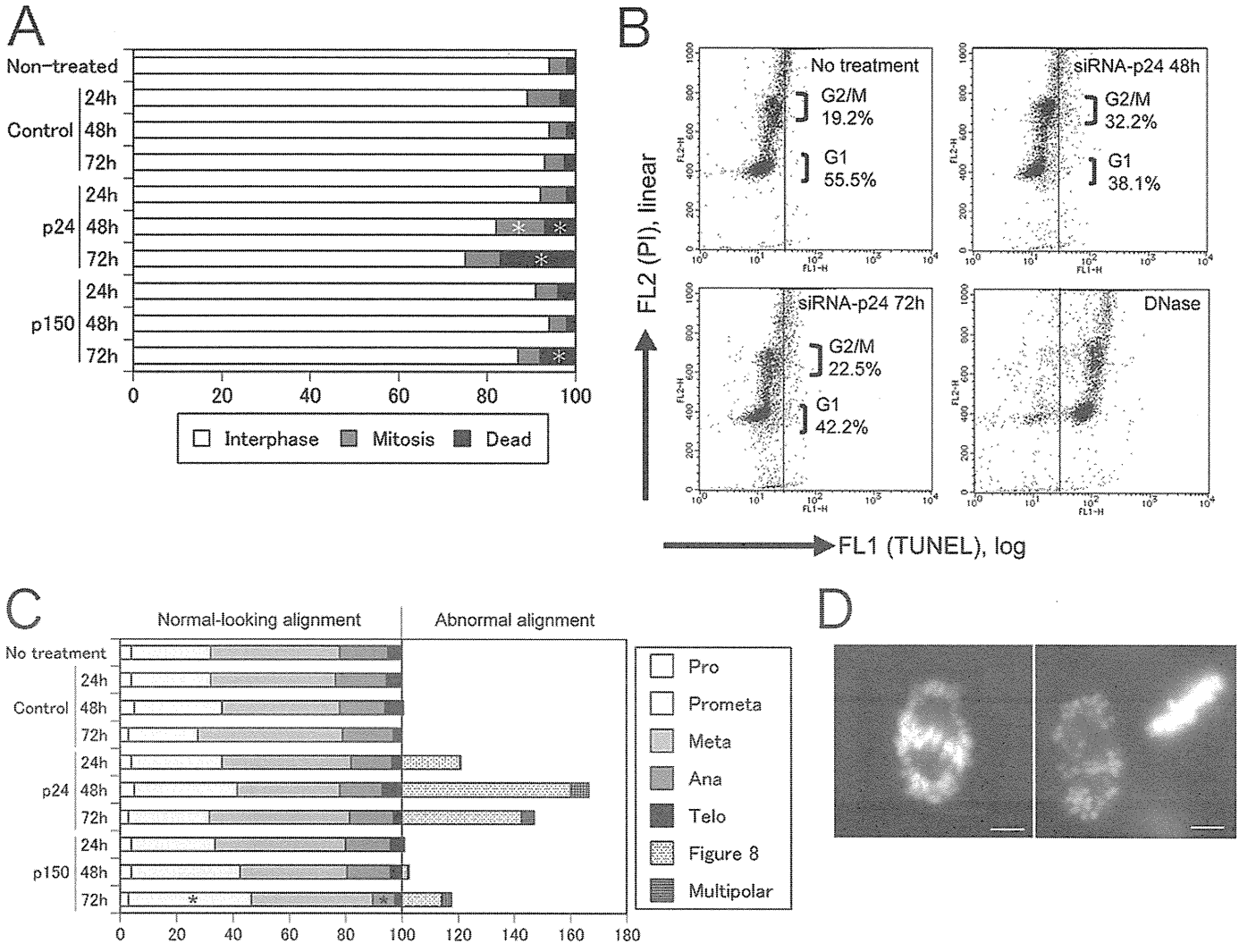

FIGURE 2. **Down-regulation of p24 and p150 induces mitotic abnormalities in HeLa(tc) cells.** *A*, cells were treated with each siRNA for periods indicated on the *left*. From a total of 300 cells counted/treatment, the relative percentages of mitotic, interphase, and dead cells determined by separation of floating cells (mitotic and dead *versus* interphase) and by trypan blue dye exclusion (live *versus* dead) are indicated by *shading*. *Asterisks* indicate a statistically significant ($p < 0.01$) increase relative to the no treatment control using Chi-square test. *B*, cells treated with siRNA-p24 for indicated periods were stained with propidium iodide (*PI*) just prior to flow cytometry and TUNEL analysis. FL1 values on the *horizontal axis* indicate the amount of dUTP polymerized by DNA free 3′ ends, whereas FL2 values on the *vertical axis* show the DNA content. *C*, from a total of 300 cells counted/treatment, the percentages of mitotic cells with normal-looking chromosome alignment (100% total) or abnormal mitosis were determined from observations of Hoechst 33342-stained nuclei. *Asterisks* indicate statistically significant changes in a particular mitotic phase ($p < 0.01$) relative to the no treatment control by Chi-square test. *D*, representative images of Hoescht 33342-stained chromosomes in a figure eight alignment. *Bar*, 5 μm. *Pro*, prophase; *Prometa*, prometaphase; *Meta*, metaphase; *Ana*, anaphase; *Telo*, telophase.

onstrate that siRNA-p24 induces mitotic delay/arrest, in that the G_2/M-phase ratio (Fig. 2*B*, *vertical axis*) was significantly higher in treated cells (32.2%) than in cells without treatment (19.2%) However, the cell death induced by siRNA-p24 does not appear apoptotic because TUNEL assays showed only a small increase in DNA free 3′ ends (Fig. 2*B*, *horizontal axis*; see DNase-treated HeLa cell panel as a positive control) in siRNA-p24-treated cells.

To determine the effects of down-regulation of p24 and $p150^{Glued}$ on mitosis, we analyzed chromosome alignment in Hoechst 33342-stained mitotic cells. Although treatment of cells with control siRNA (100 nM) for up to 72 h did not affect their distribution (Fig. 2*C*), we observed that treatment with siRNA-p24 for 48 h specifically induced one of two distinct patterns of abnormal chromosome alignment in 39.8% (133/334) of mitotic cells (Fig. 2*C*). First, chromosomes in 120 mitotic cells treated with siRNA-p24 for 48 h aligned abnormally to resemble a figure eight pattern (Fig. 2*D*), whereas the same pattern almost never appeared (<1/200) in mitotic cells without siRNA treatment or those treated with control siRNA. Second, 3.9% (13/334) of mitotic cells treated with siRNA-p24 for 48 h demonstrated multipolar mitoses. Among the remaining 201 mitotic cells with normal-looking chromosome alignment, the distribution of cells in each mitotic phase was not altered. Relative to cells treated for 48 h, cells treated with siRNA-p24 for 24 or 72 h showed the same abnormal pattern of chromosome alignment but at a lower frequency (Fig. 2*C*).

In contrast to siRNA-p24-treated cells, cells treated with siRNA-p150 for 48 h showed no significant change in distribution among mitotic phases, and only a few cells demon-

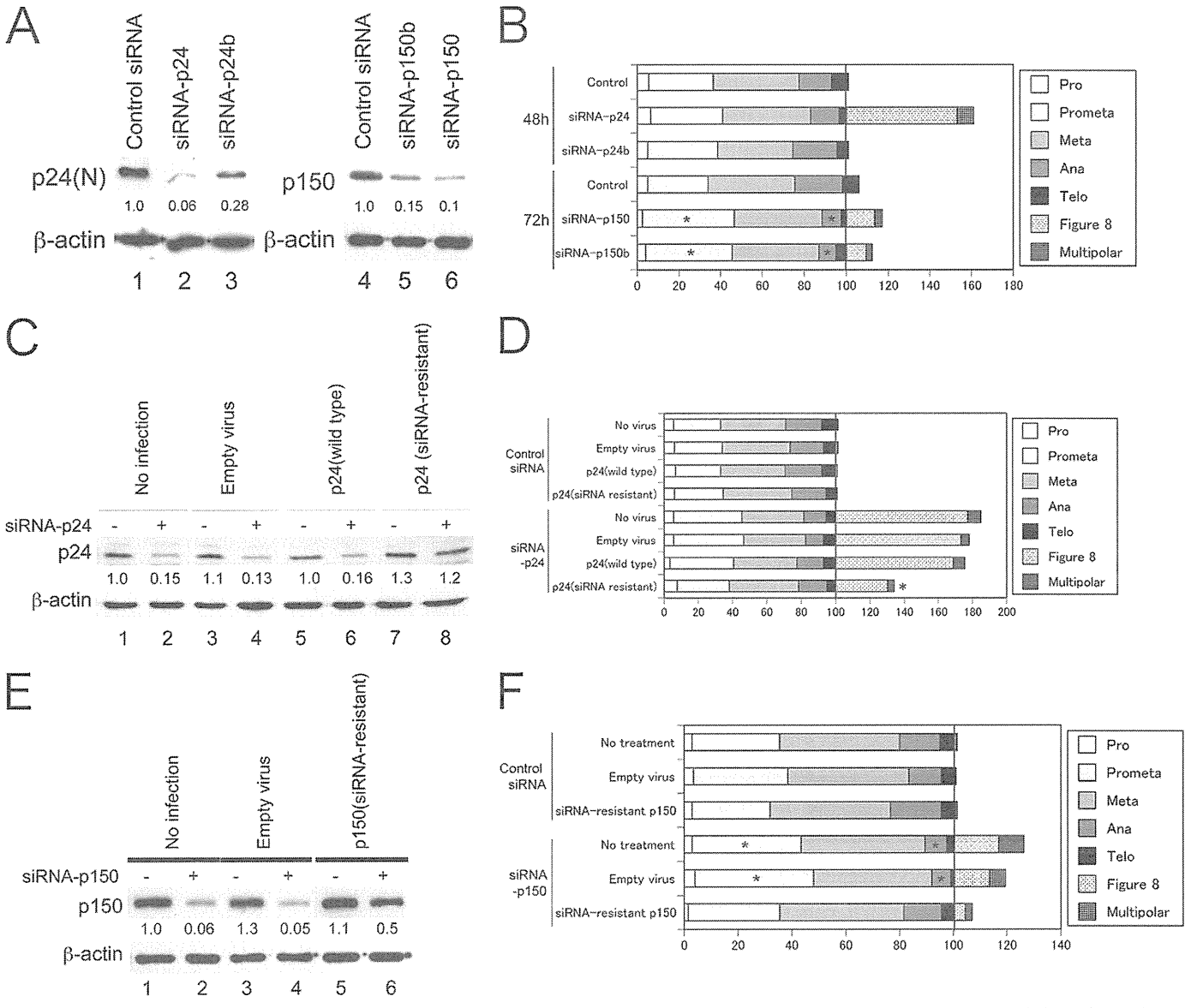

FIGURE 3. *A*, immunoblot analysis using p24(N), p150, or β-actin antibody. HeLa(tc) cells were treated with the siRNA (100 nM) indicated above for 48 (*lanes 1–3*) or 72 h (*lanes 4–6*). Ratios of signal intensity relative to actin (measured using densitometry) are indicated *below each lane*. *B*, *D*, and *F*, the percentages of mitotic cells with normal-looking chromosome alignment (100% total) or abnormal mitosis were determined from observations of Hoechst 33342-stained nuclei in a total of 300 cells/treatment. *Asterisks* indicate statistically significant changes in a particular mitotic phase ($p < 0.01$) relative to the no treatment control using the Chi-square test. *C*, immunoblot analyses using p24(N) or β-actin antibody. *Lanes 1* and *2*, uninfected HeLa(tc) cells; *lanes 3* and *4*, cells infected with empty virus; *lanes 5* and *6*, cells infected with virus containing wild type p24 cDNA; *lanes 7* and *8*, cells infected with virus containing siRNA-resistant p24 cDNA. *Lanes 1*, *3*, *5*, and *7*, cells were treated with control siRNA; *lanes 2*, *4*, *6*, and *8*, cells were treated with siRNA-p24 (100 nM) for 48 h. Ratios of relative signal intensity (p24/actin) are indicated *below each lane*. *E*, immunoblot analysis using p150 or β-actin antibody. *Lanes 1* and *2*, uninfected HeLa(tc) cells; *lanes 3* and *4*, cells infected with empty virus; *lanes 5* and *6*, cells infected with virus containing siRNA-resistant p150 cDNA. *Lanes 1*, *3*, and *5*, cells were treated with control siRNA; *lanes 2*, *4*, and *6*, cells were treated with siRNA-p150 (100 nM) for 72 h. Ratios of relative intensity (p150/actin) are indicated *below each lane*. *Pro*, prophase; *Prometa*, prometaphase; *Meta*, metaphase; *Ana*, anaphase; *Telo*, telophase.

strated the figure eight chromosome alignment seen with siRNA-p24 (Fig. 2*C*). After an additional 24 h of treatment with siRNA-p150, however, we observed a significant increase in the ratio of prometaphase cells and a corresponding decrease in anaphase and telophase cells. In addition, small percentages of mitotic cells showed the figure eight chromosomal alignment (11.9%, 28/236) or multipolar mitoses (3.0%, 7/236).

We also treated cells with secondary siRNAs that target alternative sequences in the p24 or $p150^{Glued}$ genes. When cells were treated with siRNA-p24b, which only reduced p24 levels ~3-fold (Fig. 3*A*), few mitotic cells showed the figure eight chromosome alignment (Fig. 3*B*), suggesting that greater reductions in p24 protein levels are required to induce the figure eight alignment. In contrast, cells treated with siRNA-p150b reduced p150 to levels similar to siRNA-p150 (Fig. 3*A*) and showed similar mitotic disturbances, including an increased ratio of prometaphase cells, a decreased ratio of anaphase/telophase cells, and a few cells with figure eight chromosome alignment.

To exclude the possibility that the figure eight chromosome alignment is an off-target effect of siRNA-p24, we performed

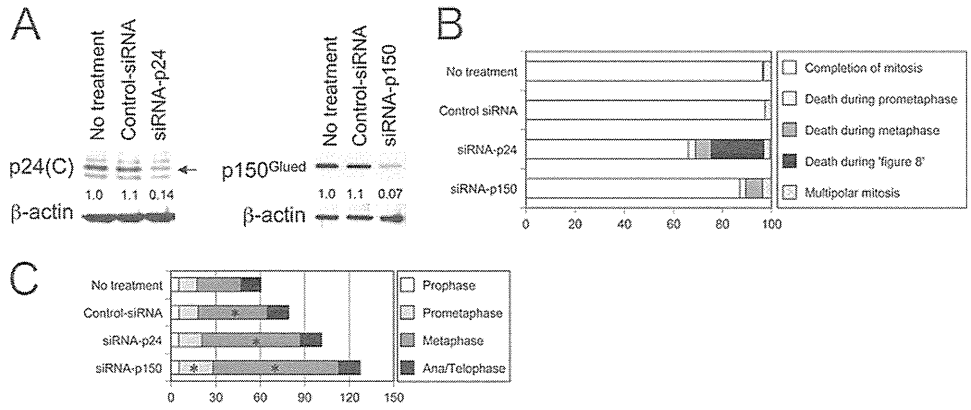

FIGURE 4. **Time-lapse observations of mitotic cells.** *A*, immunoblot analyses of lysates from U2OS cells using p24(C), p150^{Glued}, or β-actin antibody. Cells were treated with the siRNA indicated for 72 h. Ratios of relative intensity (p24 or p150/actin) measured by densitometry are indicated *below each lane*. An *arrow* marks the position of p24. *B*, U2OS cells expressing an H2B-GFP fusion protein were treated with control siRNA or siRNA-p150 for >48 h or with siRNA-p24 for >24 h. Percentages of cells demonstrating termination of mitosis in one of the manners listed on the *right* are indicated with *shading*. *C*, the average duration of each mitotic phase (min) in cells that completed mitosis are indicated by shading. *Asterisks* indicate a statistically significant increase in duration ($p < 0.05$) relative to the no treatment control.

rescue experiments by expressing a siRNA-p24-resistant p24 mRNA from a pantropic retrovirus containing EGFP as a selection marker (see "Experimental Procedures"). EGFP-positive cells were sorted using flow cytometry and then treated with siRNA-p24.

Immunoblot analyses revealed similar levels of p24 in cells infected with retrovirus containing p24 cDNA or siRNA-resistant p24 cDNA (Fig. 3*C*, *lanes 5* and *7*). Following treatment with siRNA-p24 (100 nM for 48 h), uninfected cells, as well as those infected with empty virus or virus containing wild-type cDNA (Fig. 3*C*, *lanes 2*, *4*, and *6*) showed down-regulation of p24 protein. In contrast, there was no significant reduction in p24 levels in cells expressing the siRNA-resistant p24 cDNA (Fig. 3*C*, *lane 8*). Mitotic cells with the figure eight chromosome alignment were observed in cells infected with empty virus (73%) or virus containing wild type cDNA (68.5%) at virtually the same frequency as uninfected cells (77.3%) (Fig. 3*D*). Only cells infected with virus containing the siRNA-resistant cDNA showed a significant reduction in the frequency figure eight mitoses (34.5%, $p < 0.01$), suggesting that p24 is indeed effective in preventing chromosomes from the figure eight alignment.

We also expressed a siRNA-resistant p150 cDNA in HeLa cells using the same pantropic retrovirus system (Fig. 3*E*). Unlike uninfected cells or those infected with the empty virus, cells expressing siRNA-resistant cDNA showed little decrease in p150 levels following siRNA treatment. Similarly, there was no significant increase in prometaphase or decrease in ana/telophase ratios in cells treated with siRNA-p150 (Fig. 3*F*), and the ratio of cells with the figure eight chromosome alignment decreased.

Chromosomes Align into a Figure Eight after Metaphase Arrest—To further analyze the mitotic disturbances induced by p24 or p150^{Glued} down-regulation, we established a U2OS cell line expressing a histone H2B-GFP fusion protein constitutively (19), transfected these cells with control, p24, or p150^{Glued} siRNAs (efficiency typically 70%) and then collected time-lapse images of the transfected cells. In these cells, the magnitude in reduction of p24 or p150^{Glued} protein expression levels by siRNA-p24 or siRNA-p150, respectively, were similar to those achieved in HeLa cells (Fig. 4*A*).

More than 95% of mitotic cells without siRNA treatment or treated with control siRNA completed mitosis (Fig. 4*B*, also see supplemental Movie 1). Cells treated with control siRNA demonstrated a significant elongation of metaphase (46 min in control siRNA-treated cells to compare with 29 min in untreated cells, $p < 0.05$), whereas the durations of prophase, prometaphase, and anaphase and telophase combined (ana/telophase) were not affected (Fig. 4*C*). These data suggest that U2OS cells treated with scrambled siRNA and/or cationic liposome experience a delayed progression through metaphase. Only one of 180 (0.55%) untreated cells and zero of 156 cells treated with control siRNA died while in mitosis.

When cells were treated with siRNA-p24 (100 nM) for >24 h, we observed a significant delay in metaphase (average of 66 min) relative to control siRNA-treated cells (average of 46 min, $p < 0.05$, Fig. 4*C*). There was no elongation in the duration of prometaphase or ana/telophase. We also observed cell death more frequently in siRNA-p24-treated cells: 3% (10/333) or 6.5% (22/333) of mitotic cells underwent cell death during prometaphase or metaphase, respectively (Fig. 4*B*). Intriguingly, in 21.5% (72/333) of siRNA-p24-treated mitotic cells, chromosomes aligned at the metaphase plate during prolonged metaphase broke up into a figure eight pattern (supplemental Movie 2). This similarity to the abnormal chromosome alignment observed in siRNA-p24-treated HeLa cells (Fig. 2*D*) indicates that these are not prometaphase cells but rather post-metaphasic cells that fail to enter anaphase. All 72 cells with figure eight chromosome alignment underwent cell death eventually (an average of 164 min after breakup of chromosome alignment at the metaphase plate) (supplemental Movie 2). Overall, 31% (104/333) of siRNA-p24-treated mitotic cells underwent cell death, whereas these cells in interphase rarely underwent apoptosis (< 0.1%).

In contrast to control siRNA- or siRNA-p24-treated cells, cells treated with siRNA-p150 for >48 h demonstrated delayed prometaphase (average of 23 min to compare with 12 min in control siRNA-treated cells, $p < 0.05$, Fig. 4*C*), during

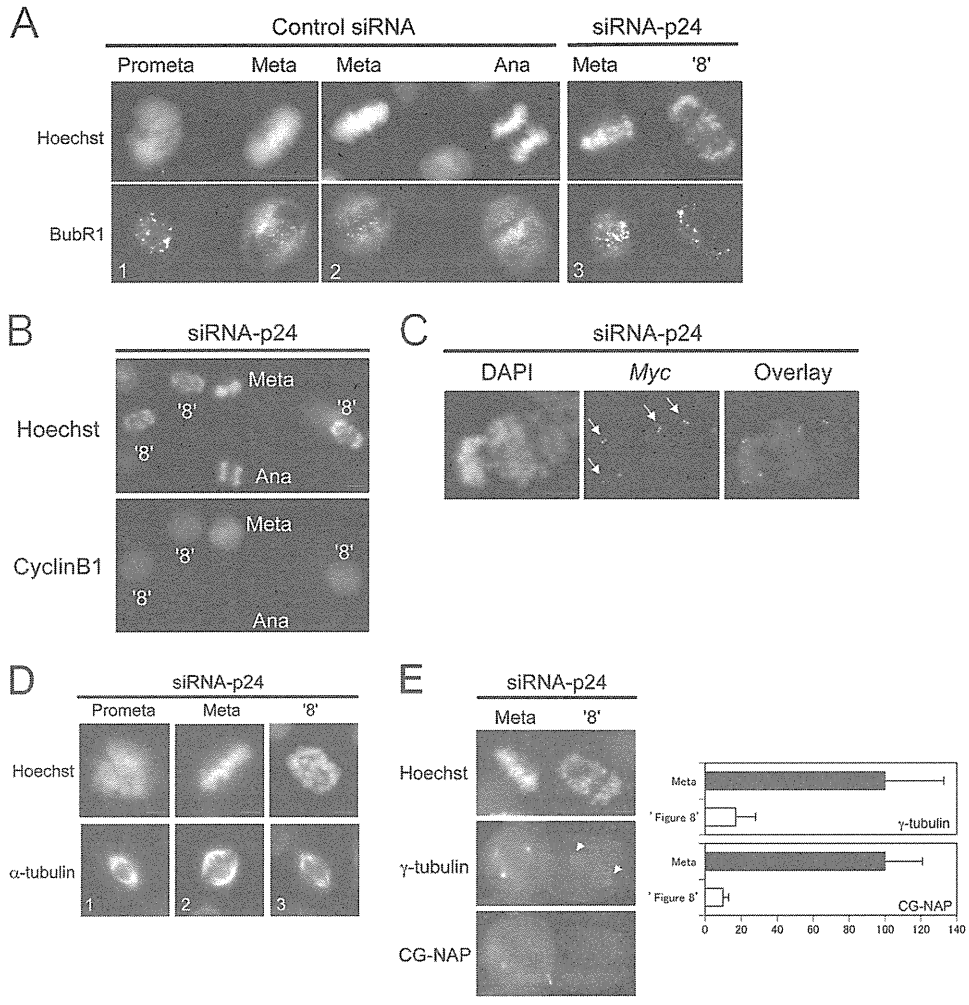

FIGURE 5. **Mechanisms of figure eight chromosome alignment.** *A*, *B*, and *D*, HeLa cells were treated with the siRNA indicated and immunostained with the antibody indicated on the *left*. DNA was stained with Hoechst 33342, and the mitotic phase of cells are labeled *above or within* each image. *Bars*, 10 μm (*A* and *B*) and 5 μm (*D*). *C*, HeLa cells treated with siRNA-p24 were fixed with formaldehyde, denatured, and hybridized with a c-*myc* probe for FISH analysis. DNA was stained with DAPI. *Arrows* mark pairs of dots that indicate sister chromatids. *Bar*, 5 μm. *E*, HeLa cells were treated with siRNA-p24 and immunostained with the antibody indicated on the *left*. Relative fluorescence intensity of proteins in either metaphase (*black bars*) or figure eight (*open bars*) centrosomes (*right panels*). The mean (+ S.D.) intensity of 50 centrosomal areas was measured, and background levels were subtracted. *Bar*, 5 μm. *Prometa*, prometaphase; *Meta*, metaphase; *Ana*, anaphase.

which 2.4% (4/163) underwent cell death. Moreover, the metaphase delay induced by siRNA-p150 (average 85 min, Fig. 4*C*, see Video 3) was more severe than in cells treated with siRNA-p24 and 6.7% (11/163) of siRNA-p150-treated mitotic cells underwent cell death during metaphase. These findings are consistent with previous experiments in which HeLa cells treated with siRNA-p150 showed increased ratios of cells in prometaphase and metaphase relative to cells in anaphase and telophase (Fig. 2*C*). Unlike cells treated with siRNA-p24, none of these mitotic cells showed chromosomes aligned in a figure eight pattern, and all cells that survived through prometaphase and metaphase entered anaphase.

Cells with Figure Eight Chromosome Alignment Share Features with Prometaphase—Our findings demonstrate that down-regulation of either p24 or $p150^{Glued}$ induces severe metaphasic delays. This phenotype is analogous to a previous report about cells that undergo metaphase arrest/delay when dynactin is depleted by dynamitin overexpression (8). In that case, the delay is most likely due to a defect in the function of the dynein-dynactin complex, which removes spindle checkpoint proteins such as BubR1 from kinetochores during metaphase (reviewed in Ref. 20). Indeed, when cells were treated with control siRNA, BubR1 signals localized to kinetochores in prometaphase (Fig. 5*A*, *panel 1*), after which the signal decreased rapidly during metaphase and anaphase (*panels 1* and *2*). In contrast, cells treated with siRNA-p24 showed the same intensity of BubR1 immunofluorescence at the kinetochores of metaphase chromosomes as that in prometaphase cells, including those cells with a figure eight chromosome alignment (*panel 3*).

Despite their similarities in appearance to prometaphase (rather than anaphase) cells, the figure eight chromosome alignment is only seen in cells that have progressed through metaphase (supplemental Movie 2). To further characterize the timing of this unique chromosomal alignment, we looked at expression of cyclin B1, a molecule that is present during metaphase (Fig. 5*B*, *Meta*) and then degraded rapidly in anaphase (*Ana*). We observed positive cyclin B1 immunofluorescence in all mitotic cells with a figure eight chromosome alignment. Moreover, FISH images of the c-*myc* gene on

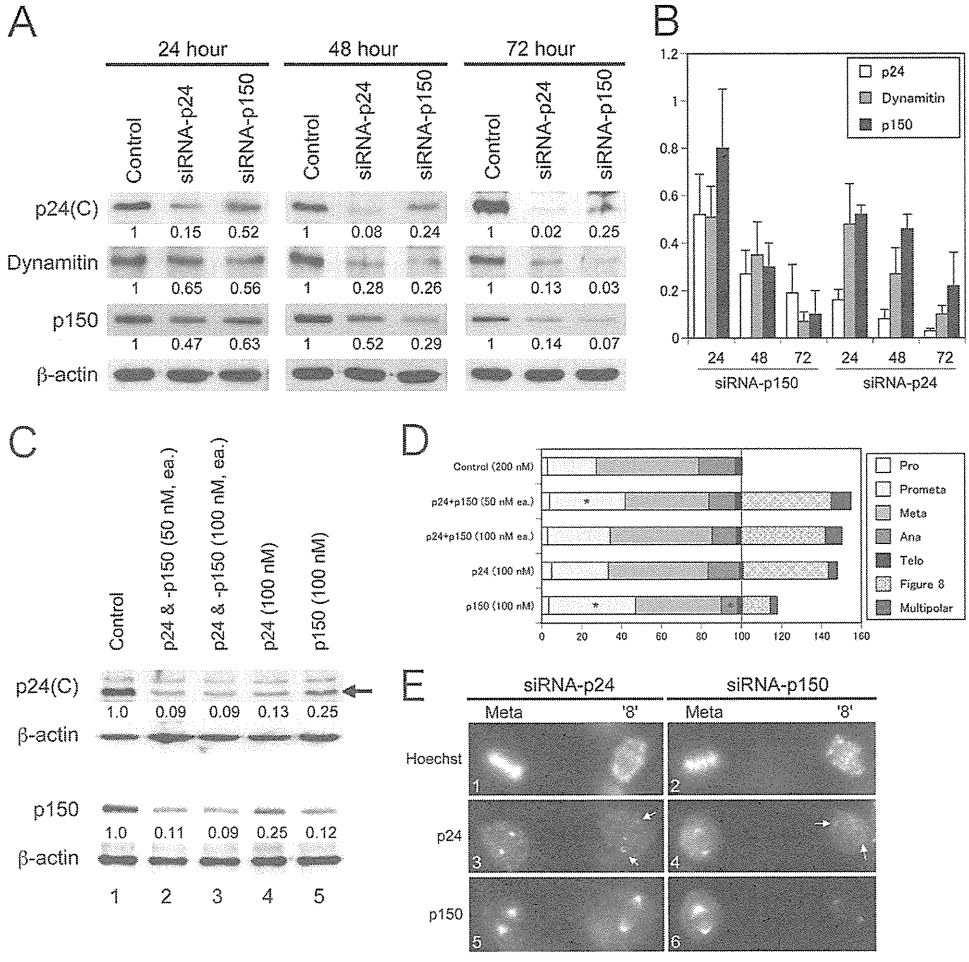

FIGURE 6. **p24 expression levels relate to figure eight configuration.** *A* and *C*, immunoblot analyses using p24(C), dynamitin, p150^{Glued}, or β-actin antibody. HeLa cells were treated with siRNA (100 nM, otherwise indicated) as indicated above for 72 h. Ratios of relative intensity (p24, dynamitin, or p150 actin) measured by densitometry are indicated *below each lane*. Data are representative of four independent experiments that yielded similar results. *B*, average and S.D. protein expression levels in four independent experiments of p24, dynamitin, and p150^{Glued} relative to control siRNA-treated cells. *D*, HeLa (tc) cells were treated with the siRNA indicated on the *left* for 72 h. From a total of 300 cells counted/treatment, the percentages of mitotic cells with normal-looking chromosome alignment (100% total) or abnormal mitosis were determined from observations of Hoechst 33342-stained nuclei. *Asterisks* indicate statistically significant changes in a particular mitotic phase ($p < 0.01$) relative to the no treatment control using a Chi-square test. *E*, HeLa cells were treated with the siRNA indicated above and immunostained with the antibody indicated on the *left*. DNA was stained with Hoechst 33342, and the mitotic phase of each cell is labeled *above*. *Bar*, 10 μm. *Pro*, prophase; *Prometa*, prometaphase; *Meta*, metaphase; *Ana*, anaphase; *Telo*, telophase. '8', figure eight.

chromosome band 8q24 indicate that sister chromatids in cells with figure eight alignment have yet to segregate because four pairs of dots are visible on chromosomes in figure eight cells (Fig. 5*C*, *arrows*; FISH with chromosome 8-specific centromeric probes revealed that HeLa(tc) cells have four chromosome 8 (data not shown)). These data suggest that cells with figure eight chromosome alignment are most like prometaphase cells.

Because the alignment of chromosomes on the metaphase plate is mediated by tension between the spindle poles, reversal of the mitotic process by siRNA-p24 interference may be due to reductions in spindle tension. Using α-tubulin immunostaining, we compared the density and morphology of spindles in cells at different stages of mitosis. In cells displaying a figure eight configuration (Fig. 5*D*, *panel 3*), the robust fluorescence characteristic of metaphase mitotic spindles (*panel 2*) reverted to a shape and intensity more characteristic of mitotic spindles in prometaphase (*panel 1*). Moreover, the marked decrease in immunostaining signal intensity for γ-tubulin and CG-NAP (pivotal components of the γ-tubulin ring complex that provides microtubule nucleation sites) in figure eight-stage cells relative to metaphase cells (Fig. 5*E*) suggests that p24 is required to maintain the integrity of metaphase centrosomes.

p24 Levels Relate to Figure Eight Chromosome Alignment—In parallel experiments conducted in two different cell lines (HeLa or U2OS), metaphase arrest/delay was induced similarly following treatment with either siRNA-p24 or siRNA-p150; however, siRNA-p24 was significantly more effective than siRNA-p150 in inducing the figure eight chromosome alignment during metaphase (Figs. 2*C* and 4, *B* and *C*). We did not observe any change in expression of p150^{Glued} and p24 mRNAs following treatment with siRNA-p24 or siRNA-p150, respectively (Fig. 1*A*). However, both of these siRNAs did reduce protein expression levels of p24, p150^{Glued}, and dynamitin in HeLa(tc) cells (Fig. 6*A*). Similar results were obtained in U2OS cells (data not shown). Similar to previous reports demonstrating that overexpression of dynamitin disrupts dynactin structure (2), our results with p24 and p150^{Glued} suggest that balanced availability of all

components is required to maintain the stability of the dynactin complex.

To test whether changes in p24 expression levels are sufficient to induce the figure eight chromosome alignment, we treated cells with siRNAs and then measured the expression levels of dynactin components and observed alterations in chromosome alignment. When cells were treated with siRNA-p150 for 24 or 48 h, expression levels of p24, dynamitin, and p150^{Glued} relative to control cells were ~25% or higher (Fig. 6*B*), but no mitotic abnormalities were observed (Fig. 2, *A* and *C*). Treatment with siRNA-p150 for 72 h reduced the expression levels of dynamitin and p150^{Glued} to <10% and p24 to ~20%, and this treatment induced metaphase arrest/delay and a few cells with the figure eight chromosome alignment (Fig. 2*C*). In contrast, treatment of cells with siRNA-p24 for 24 or 48 h reduced the expression levels of p24 to less than 15%, while maintaining relatively high (>25%) levels of dynamitin and p150^{Glued}. In this case, more mitotic cells showed a figure eight chromosome alignment (Fig. 2*C*).

We also treated HeLa(tc) cells with a combination of both siRNA-p24 and siRNA-p150 (50 or 100 nM each) for 72 h. Although this procedure reduced both p24 and p150 expression levels to ~10% of those in control cells (Fig. 6*C*, *lanes 2* and *3*), the ratio of cells in the figure eight alignment (42–45%) was virtually the same as cells treated with siRNA-p24 alone (43%, Fig. 6*D*), in which p24 and p150 expression are reduced to ~10 and 25% of control cells, respectively (Fig. 6*C*, *lane 4*). Once again, cells treated with siRNA-p150 alone that expressed p24 at 25% and p150 at 10% of control cells (*lane 5*) showed only a small number (~10%) of mitotic cells with the figure eight configuration (Fig. 6*D*). These data demonstrate that among all components of the dynactin complex, manipulation of p24 expression levels is most likely to result in cells assuming the figure eight configuration.

Further evidence in support of this correlation was observed when treated cells were immunostained simultaneously for p24 and p150^{Glued}. p24 immunofluorescence at centrosomes of mitotic HeLa(tc) cells treated with siRNA-p24 was markedly less intense in cells with the figure eight chromosome alignment relative to metaphasic cells in the same microscopic field (Fig. 6*E*, *panel 3*). Intriguingly, p150 immunofluorescence at centrosomes in most (23/25) of these figure eight cells was as bright as the signal in metaphasic cells (Fig. 6*E*, *panel 5*). In contrast, in cells treated with siRNA-p150, both p24 and p150 immunofluorescence signals in figure eight cells were markedly reduced (Fig. 6*E*, *panels 4* and *6*) in all cells observed (25/25). These results suggest that failure of p24 to accumulate in mitotic centrosomes induces figure eight chromosome alignment.

DISCUSSION

In this report, we treated HeLa and U2OS cells with siRNAs specific for p24 or p150^{Glued}, two components of the projecting arm of the dynactin complex. Time-lapse observations reveal that treatment of siRNA-p24 induces severe metaphase delay. In >40% of metaphase cells struggling to enter anaphase, chromosomes aligned on the metaphase plate break away and assume a configuration resembling a figure eight. In time, all cells with the figure eight alignment die without completing mitosis. In contrast with p24, cells treated with siRNA-p150 demonstrate severe delays in metaphase, but most cells do not assume the figure eight alignment and ultimately progress to anaphase. Neither p24 nor p150^{Glued} appears to be involved in the progression of anaphase and telophase.

Reductions in p24 or p150^{Glued} protein levels induce metaphase arrest/delay (Fig. 4*C* and supplemental Movies 1–3). This is consistent with a previous report in which cells overexpress dynamitin, which down-regulates dynactin function, also undergo metaphase arrest/delay (8). Failure to remove spindle checkpoint proteins such as BubR1 from kinetochores (Fig. 5*A*) results in metaphase delay because checkpoint proteins inhibit cdc20, a specific activator of the anaphase-promoting complex/cyclosome (reviewed in Ref. 20). Because anaphase-promoting complex/cyclosome functions as an E3 ubiquitin ligase, mitotic checkpoint proteins that are remain on kinetochores delay ubiquitin-dependent degradation of cyclin B1 (Fig. 5*B*) or securin, which then inhibits cohesin hydrolysis and blocks chromosome segregation (Fig. 5*C*).

Nonetheless, the transition of chromosomes from a metaphase to a figure eight configuration does not appear to be a direct result of spindle checkpoint protein retention at kinetochores. Because there is a marked reduction of γ-tubulin and CG-NAP signals at mitotic centrosomes in cells with the figure eight chromosome alignment (Fig. 5*E*), insufficient amounts of γ-TuRC in metaphase centrosomes appear to be one of the major factors driving the phenotype. Thus, we hypothesize that loss of spindle microtubule tension (Fig. 5*D*) is the defect that induces chromosomes to break away from alignment at the metaphase plate.

The two functions of the dynactin complex are to remove spindle checkpoint proteins from kinetochores and to maintain centrosome integrity until entry into anaphase. Although we have observed that neither of these functions are disturbed when expression levels of p24, dynamitin, or p150^{Glued} remain at least 25% of control levels (siRNA-p150 for 48 h, see Figs. 2*C* and 6*A*), we did note that a 10-fold reduction in the expression of either p24 or p150^{Glued} impaired the removal of checkpoint proteins, resulting in metaphase delay. In contrast, chromosome integrity and the resulting formation of figure eight cells was only induced with a 10-fold reduction in p24 levels but not with a reduction in p150^{Glued}. Immunofluorescence experiments also emphasized a correlation between accumulation of p24 (but not p150^{Glued}) in centrosomes and figure eight chromosome alignment (Fig. 6*E*). These data suggest that p24 acts independently of p150^{Glued} in metaphase centrosomes, where it helps maintain chromosome integrity and prevents breakaway until entry into anaphase.

Although it is generally accepted that p24, dynamitin, and p150^{Glued} function together in the dynactin projecting arm (2), we and others (4, 21) have observed that the localization of different dynactin components during mitosis varies considerably. For example, p24 immunofluorescence is strong at centrosomes relative to mitotic spindles or kinetochores. This is particularly evident during early anaphase (Fig. 1, *E* and *F*)

when p150^{Glued} immunofluorescence is barely detectable. In conclusion, our results suggest that p24 operates independently from the dynactin complex in binding to metaphase centrosomes and maintaining their integrity. To explore this hypothesis further, we are currently investigating the function of p24 in metaphase centrosomes in greater detail.

Acknowledgments—We thank Dr. K. Kevin Pfister (University of Virginia) for kindly providing antibodies against p24, Dr. M. Katsuno and G. Sobue (Nagoya University) for providing expression vectors for p150^{Glued}, and M. Nakamura for excellent technical assistance.

REFERENCES

1. Musacchio, A., and Salmon, E. D. (2007) *Nat. Rev. Mol. Cell Biol.* **8,** 379–393
2. Schroer, T. A. (2004) *Annu. Rev. Cell Dev. Biol.* **20,** 759–779
3. Pfister, K. K., Benashski, S. E., Dillman, J. F., 3rd, Patel-King, R. S., and King, S. M. (1998) *Cell Motil Cytoskeleton* **41,** 154–167
4. Karki, S., LaMonte, B., and Holzbaur, E. L. (1998) *J. Cell Biol.* **142,** 1023–1034
5. Eckley, D. M., and Schroer, T. A. (2003) *Mol. Biol. Cell* **14,** 2645–2654
6. Amaro, I. A., Costanzo, M., Boone, C., and Huffaker, T. C. (2008) *Genetics* **178,** 703–709
7. Burkhardt, J. K., Echeverri, C. J., Nilsson, T., and Vallee, R. B. (1997) *J. Cell Biol.* **139,** 469–484
8. Whyte, J., Bader, J. R., Tauhata, S. B., Raycroft, M., Hornick, J., Pfister, K. K., Lane, W. S., Chan, G. K., Hinchcliffe, E. H., Vaughan, P. S., and Vaughan, K. T. (2008) *J. Cell Biol.* **183,** 819–834
9. Cheung, P. Y., Zhang, Y., Long, J., Lin, S., Zhang, M., Jiang, Y., and Wu, Z. (2004) *J. Biol. Chem.* **279,** 45308–45311
10. Dixit, R., Levy, J. R., Tokito, M., Ligon, L. A., and Holzbaur, E. L. (2008) *J. Biol. Chem.* **283,** 33611–33619
11. Oshimori, N., Ohsugi, M., and Yamamoto, T. (2006) *Nat. Cell Biol.* **8,** 1095–1101
12. Katsuno, M., Adachi, H., Minamiyama, M., Waza, M., Tokui, K., Banno, H., Suzuki, K., Onoda, Y., Tanaka, F., Doyu, M., and Sobue, G. (2006) *J. Neurosci.* **26,** 12106–12117
13. Soneoka, Y., Cannon, P. M., Ramsdale, E. E., Griffiths, J. C., Romano, G., Kingsman, S. M., and Kingsman, A. J. (1995) *Nucleic Acids Res.* **23,** 628–633
14. Burns, J. C., Friedmann, T., Driever, W., Burrascano, M., and Yee, J. K. (1993) *Proc. Natl. Acad. Sci. U.S.A.* **90,** 8033–8037
15. Kuribara, R., Kinoshita, T., Miyajima, A., Shinjyo, T., Yoshihara, T., Inukai, T., Ozawa, K., Look, A. T., and Inaba, T. (1999) *Mol. Cell. Biol.* **19,** 2754–2762
16. Kuribara, R., Honda, H., Matsui, H., Shinjyo, T., Inukai, T., Sugita, K., Nakazawa, S., Hirai, H., Ozawa, K., and Inaba, T. (2004) *Mol. Cell. Biol.* **24,** 6172–6183
17. Tokai-Nishizumi, N., Ohsugi, M., Suzuki, E., and Yamamoto, T. (2005) *Mol. Biol. Cell* **16,** 5455–5463
18. Shinjyo, T., Kuribara, R., Inukai, T., Hosoi, H., Kinoshita, T., Miyajima, A., Houghton, P. J., Look, A. T., Ozawa, K., and Inaba, T. (2001) *Mol. Cell. Biol.* **21,** 854–864
19. Shi, Q., and King, R. W. (2005) *Nature* **437,** 1038–1042
20. Lu, Y., Wang, Z., Ge, L., Chen, N., and Liu, H. (2009) *Cell Struct. Funct.* **34,** 31–45
21. Echeverri, C. J., Paschal, B. M., Vaughan, K. T., and Vallee, R. B. (1996) *J. Cell Biol.* **132,** 617–633